Politecnico di Torino

Politecnico di Torino

Corso di Laurea Magistrale in Ingegneria dei Materiali

Collegio di Ingegneria Chimica e dei Materiali

A.A. 2023/2024

Sessione di Laurea Luglio 2024

Synthesis of hybrid polymer/liquid electrolytes for lithium-ion batteries

Polymerization-induced phase separation of electrolytes into bicontinuous structures suitable for lithium-ion batteries

Relatori:

Prof. Marco Sangermano

Prof. Mats K.G. Johansson

Candidato:

Gabriele Maffeis

Abstract

In recent years, due to the increased sensitivity towards the theme of sustainability, lithium-ion batteries have grown interest as well-established potential solutions for replacing fossil fuels. For this reason, different ways to optimize battery technologies have been covered. One idea is based on the concept of massless energy storage and is represented in practice by structural lithium-ion batteries, multifunctional systems that provide satisfying electrochemical and thermomechanical properties at the same time. The basic components of batteries have been redesigned. Electrodes made of carbon fibres are now at an advanced stage of research, while the electrolyte has not been optimized yet. Bicontinuous electrolytes have been obtained through polymerization-induced phase separation to ensure appreciable ionic conductivity and stiffness, thanks to the cooperative work of the polymer network and the liquid percolating phase. Reaction kinetics, thermodynamic of mixing and physical properties have been related to each other to define whether it is possible to predict the morphology of the electrolyte, which is responsible for providing the required properties. Even though the mechanisms are complex, and the intervening variables are interconnected, relevant conclusions can be presented. Particularly, it is underlined the synergetic effect of the constituting monomers in copolymers in enhancing ionic conductivity. Moreover, a gradual transition between percolating structures and gels was experienced, suggesting that mixed bicontinuous-gel structures could be explored as potential solutions for certain applications. The present research aims to provide understanding for further studies in the field.

Acknowledgements

The achievement of the results presented in this project has been possible thanks to the collaboration between KTH Royal Institute of Technology and Polytechnic University of Turin within the Erasmus+ program. I am grateful to Erasmus+ and the Polytechnic of Turin for giving me the possibility to complete my double degree abroad and for supporting me through a scholarship.

I would thank my supervisors Samuel Emilsson and Martina Cattaruzza for their passion in guiding me through this interesting topic. I admit that, among frequent highs, I experienced some lows, but Samuel and Martina never stopped supporting me, especially when I needed to regain motivation. Prof. Mats K.G. Johansson inspired me thanks to his professionality when I lacked new ideas. I would thank my supervisor at the Polytechnic University of Turin, prof. Marco Sangermano, who followed my progress from the Polytechnic of Turin and gave me valuable advice.

My parents, Arianna and Emanuele, my brother Nicola, my grandparents and my whole family deserve a special mention because they made me feel proud of what I have built during my academic career.

List of Figures

List of Tables

List of abbreviations

AIBN	2,2'-Azobis(2-Methylpropionitrile)
ATR	Attenuated Total Reflectance
BA1	Bisphenol A Ethoxylate (EO=1) Diacrylate
BA2	Bisphenol A Ethoxylate (EO=2) Diacrylate
BA4	Bisphenol A Ethoxylate (EO=4) Diacrylate
BDDA	1,4-Butanediol Diacrylate
BIB	Broad Ion Beam
BMA	Bisphenol A Ethoxylate (EO=2) Dimethacrylate
BMA-co-BA1	Bisphenol A Ethoxylate (EO=2) Dimethacrylate/(EO=1) Diacrylate Copolymer
BMA-co-BA2	Bisphenol A Ethoxylate (EO=2) Dimethacrylate/(EO=2) Diacrylate Copolymer
BMA-co-BA4	Bisphenol A Ethoxylate (EO=2) Dimethacrylate/(EO=4) Diacrylate Copolymer
BSE	Back-Scattered Electrons
CB	Carbon Black
CF	Carbon Fibers
CNT	Carbon Nanotube
CRM	Critical Raw Material
CTE	Coefficient of Thermal Expansion
DMA	Dynamic Mechanical Analysis
DSC	Differential Scanning Calorimetry
EC	Ethylene Carbonate
EIS	Electrochemical Impedance Spectroscopy
EO	Oxyethylene Group
FRP	Fiber-Reinforced Polymer
FTIR	Fourier-Transform Infrared Spectroscopy
HE	Hybrid Solid-Liquid Electrolyte
H-NMR	Hydrogen Nuclear Magnetic Resonance
IR	Infrared

LCM	Liquid Composite Moulding
LE	Liquid Electrolyte
LFP	$LiFePO_4$
LIB	Lithium-Ion Battery
LiTFSI	Lithium Bis(Trifluoromethanesulfonyl)Imide
NIPS	Nonsolvent-Induced Phase Separation
NMC	$LiMnNiCoO_2$
PAN	Polyacrylonitrile
PC	Propylene Carbonate
PCL	Polycaprolactone
PEG	Poly(Ethylene Glycol)
PEGDA	Poly(Ethylene Glycol) Diacrylate
PEO	Poly(Ethylene Oxide)
PIPS	Polymerisation-Induced Phase Separation
PP	Polypropylene
PTMC	Poly(Trimethylene Carbonate)
RT-FTIR	Real Time Fourier-Transform Infrared Spectroscopy
SE	Secondary Electrons
SEI	Solid Electrolyte Interphase
SEM	Scanning Electron Microscope
SPE	Solid Polymer Electrolyte
STD	Standard Deviation on the Average
TGA	Thermogravimetric Analysis
TIPS	Temperature-Induced Phase Separation
UCST	Upper Critical Solution Temperature
UV	Ultraviolet
ZRA	Zero Resistance Amperometry

List of symbols

A	Cross-sectional area (mm^2)
E	Young's modulus (MPa)
E'	Storage modulus (MPa)
E''	Loss modulus (MPa)
e	Elementary charge, $e=1.6\cdot10^{-19}$ C
j	Current (A)
k_{ij}	Rate constant of j-species to add on a i-radical
l	Length (mm)
M_c	Crosslinking averaged molecular weight (g/mol)
M_w	Weight averaged molecular weight (g/mol)
N	Number of samples analyzed (-)
n	Volumetric molecular density (m^{-3})
p	Pressure (Pa)
R	Universal gas constant, R=8.314 J/(mol·K)
R_Ω	Resistance (Ω)
r_i	Reactivity ratio of the i-species
T	Temperature
T_g	Glass transition temperature (°C)
t	Time (s)
Z	Impedance (Ω)
ε	Strain (-)
η	Viscosity (Pa·s)
λ	Wavelength (cm^{-1})
μ	Mobility ($m^2/(V\cdot s)$)
ρ	Bulk density (kg/m^3)
σ_{av}	Average ionic conductivity (S/cm)
σ_i	Ionic conductivity of the i-sample (S/cm)

τ	Shear stress (MPa)
ψ	Voltage (V)
ω	Frequency (s^{-1})

Table of contents

1. Introduction

The present study aims to compare different hybrid polymer-liquid electrolytes (HEs) based on polymerization-induced phase separation (PIPS), using monomers that have not been widely analyzed before, since previous studies mostly focused on bisphenol A ethoxylate dimethacrylate (BMA), with two oxyethylene (EO) units between each side of the bisphenol and the methacrylate groups. State-of-the-art research in batteries is presented in Chapter 1, then the field is narrowed to lithium-ion batteries (LIBs), and eventually, structural LIBs are treated with a description of the components requested. Moreover, PIPS is described according to the variables influencing the reaction and the final morphology.

Acrylates and methacrylate-acrylate copolymers have been compared to BMA regarding electrochemical and thermomechanical properties, as well as morphology, to investigate their feasibility for working structural LIBs. The project has been organized in steps to discuss each chosen feature of the HEs separately.

Characterization is performed through the experimental techniques presented in Chapter 2. Synthesis was performed inside a glovebox to limit the effects of moisture and oxygen on HE stability. Curing was conducted in an oven at 90 °C for 45 minutes, and conversion was analyzed by Fourier-transform infrared spectroscopy (FTIR), while the polymerization rate was monitored by real-time FTIR (RT-FTIR). The main characterization technique was electric impedance spectroscopy (EIS), which, more than other techniques, was useful to establish the suitability of electrolytes for any type of battery. Moreover, since structural batteries require stiff and mechanically resistant electrolytes, dynamic mechanical analysis (DMA) was conducted to define their thermomechanical properties at the desired temperatures and predict their behavior during service. Morphology was evaluated through qualitative observation, but this rough estimation was later verified by scanning electron microscopy (SEM).

BMA was first compared with the respective acrylate, named bisphenol A ethoxylate (EO=2) diacrylate (BA2). This distinction allowed for the evaluation of the effect of the methyl group on the electrolyte properties and it is extensively discussed in Chapter 3.

Then, other pure acrylates, bisphenol A ethoxylate (EO=1) diacrylate (BA1) and bisphenol A ethoxylate (EO=4) diacrylate (BA4), were studied to define the contribution of the EO group when the chain is shortened or extended, and an overview can be found in Chapter 4.

Lastly, the respective copolymers, constituted by BMA/BA1 50/50 wt% (BMA-co-BA1), BMA/BA2 50/50 wt% (BMA-co-BA2), and BMA/BA4 50/50 wt% (BMA-co-BA4), were synthesized and characterized, and results are summarized in Chapter 5.

A comprehensive overview of all tested samples is provided in Chapter 6. Other parameters, such as solvent composition and concentration, alternative monomer structures, and copolymer composition, could be considered in further research, but are not addressed here.

For complete characterization, electrolytes must be integrated into pouch cells to prove their cycling performance when the battery is repeatedly charged and discharged. Pouch cells are stacks of a nickel current collector, a HE-vacuum-infused $LiFePO_4$ (LFP) commercial cathode, a commercial separator, a lithium metal anode, and an aluminum current collector, embedded in a square aluminum bag. It was not possible to test the cycling performance of the most promising HEs that resulted from the characterization techniques mentioned, but this can become a target for future research in the field. Pouch cell manufacturing is described in chapter 7, including relevant considerations about challenges encountered when working with such sensitive materials.

Batteries are still a discussed subject because they are blamed for not being as eco-friendly as the market and the governments make people believe. Batteries employ critical raw materials (CRMs) and are not yet recyclable, but they are the most feasible solution so far to drive mobility toward a more virtuous pathway where electric energy exceeds fossil fuels. Chapter 8 is dedicated to revealing current advancements in biobased and biodegradable components for batteries, such as those derived from biomass waste.

1.1. Context

Nowadays, the world population is experiencing concerns related to climate change and its consequences. Studies have shown a correlation between human activities and environmental modification. Therefore, the need for a change towards a more conscious use of resources has risen, as evidenced by several agreements signed by governments, such as the decision to outlaw the traditional fuel engine production by 2035 in the European Union [1]. These agreements are gradually tightening regulations on production and products to achieve the goal of carbon neutrality within a reasonable interval of time. The quest for a sustainable future is led by the transportation industry and requires a shift towards electric mobility to replace fossil-powered engines. This explains why batteries have lately been growing interest as devices for energy storage. LIBs are well-established pioneering systems for this purpose, even though new concepts have been developed in the last few years to overcome some limits of such batteries.

The concept of battery as an electrochemical device for storage energy was defined during the nineteenth century for the first time. Volta is considered the pioneer, thanks to the creation, in 1799, of a stack of alternated zinc and silver layers separated by a tissue impregnated with sodium chloride. In 1866, it was

the turn of Leclanché to demonstrate that a zinc anode, coupled with a manganese oxide–carbon cathode, could produce electricity when soaked into an ammonium chloride aqueous solution. The lead–acid rechargeable battery had already been developed by Plantè a few years before, in 1859, and his discovery inspired Jungner, who explored the nickel-cadmium battery in 1901 [2]. The research in the field stopped during the first decades of the twentieth century, but it rose again more massively when electronic goods became available to a larger percentage of the population and power applications more requested [2, 3]. The variety of available batteries multiplied ever since, and now there is plenty of choice. However, the most used type so far is represented by LIBs, which provide energy storage both to electronics and electric vehicles. They represent a milestone today, thanks to the work of John Goodenough, Stanley Whittingham, and Akira Yoshino, who won the Nobel Prize in Chemistry in 2019. This technology is based on intercalation materials for electrodes. Such materials consist of layered structures where lithium ions can be housed without compromising the integrity of the cathode or affecting the electronic neutrality [2].

Energy density and specific energy, *i.e.*, the amount of energy stored per unit volume (in Wh/m^3) and the amount of energy per unit mass (in Wh/g), respectively, are the parameters that count the most in batteries. These two parameters are not necessarily dependent on each other, since they differ according to the bulk density (ρ), defined as mass per unit volume, of the battery itself. There is no need to say that high values of energy density and specific energy are desirable, indeed the most interesting materials from an engineering point of view are in the upper right corner of Figure 1.1. For clarification, energy is determined by the product of voltage (in V) and capacity (in Ah). Voltage is the potential difference between the electrodes, while capacity is the amount of charge that can flow during a complete charge/discharge cycle and is proportional to the number of ions that can be stored in the electrodes.

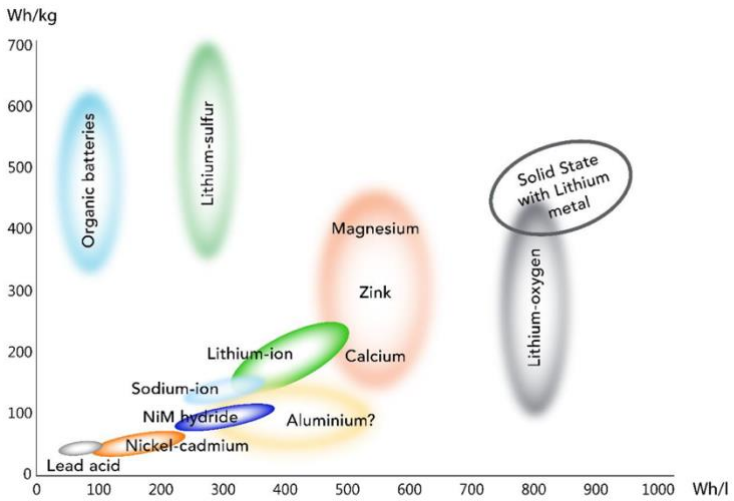

Figure 1.1. Chart representing different types of batteries with respect to their specific energy and energy density. Adapted from [4].

Among the broad variety of batteries available, LIBs show a good combination of energy storage properties and feasibility, since they are well-established in the market. Instead, lithium-sulfur and lithium-oxygen batteries, even though they look more promising on paper, are still at their first stage of development, and the same can be said for sodium-ion and aluminum-ion batteries, while lithium metal batteries (LMBs) show some risks of short circuits and depletion of performance after the formation of dendrites [5].

1.2. Structural batteries

Since LIBs are massively used in transportation, where weight is critical, researchers reflected on a way to integrate batteries into the load-bearing structure of vehicles and started to develop multifunctional materials. Such materials are expected to provide different and somehow competing properties at the same time [6], which would not be possible to achieve without a deep engineering redesign of all the components. Structural batteries represent a concept of LIBs whose purpose is to provide massless electric energy, meaning that they are made of lightweight materials featuring high mechanical properties, which would replace structural components made of metal alloys. A multidisciplinary approach disclosed similarities and compatible functionalities between intercalating electrode materials and fiber-reinforced polymer (FRP) composites.

1.2.1. Electrolyte

Liquid electrolytes (LEs) are appreciated for their high ionic conductivity values up to 10^{-2} S/cm [7-10] when they are not demanded mechanical requirements, but they are flammable when they leak out and they do not counteract detrimental chemical reactions like dendrite growth, that in severe cases is responsible for catching fire. Solid polymer electrolytes (SPEs), on the other hand, can count on Young's modulus higher than 100 MPa [11], but they do not exceed 10^{-5} S/cm ionic conductivity [12] and are most frequently in the order of 10^{-6} S/cm [9, 13]. Gel polymer electrolytes (GPEs) are intermediate between these two classes since they are featured by polymers softened by a plasticizing solvent and conduct ions almost as much as LEs (~10^{-2} S/cm), but they also have a certain extent of shape retain [9].

One of the most common SPEs, poly(ethylene oxide) (PEO), is semicrystalline at room temperature and must overcome a threshold temperature of 60 °C before it becomes amorphous and can carry ions [9]. Between the two phases that form in PEO mixed with lithium bis(trifluoromethanesulfonyl)imide (LiTFSI), the complex PEO_6:LiTFSI is more responsible for creating a tortuous path with respect to the pure PEO phase. In the eutectic region, the two aforementioned phases are dependent on each other, because the salt present in pure PEO is depleted and concentrated in the PEO_6:LiTFSI phase. Instead, at a composition different from the eutectic, the nucleation of PEO can be favored against PEO_6:LiTFSI, and higher but not satisfactory ionic conductivities can be achieved [14]. Some researchers found good perspectives for solid electrolytes using polycaprolactone (PCL)/poly(trimethylene carbonate) (PTMC)

copolymer with ceramic particles introduced as additives, namely titanium dioxide and alumina [15]. These nanoparticles inhibit crystallization, thus increasing the ionic conductivity at 25 °C by one order of magnitude with respect to virgin PCL, up to $7 \cdot 10^{-6}$ S/cm. Nanoparticles have a great impact on electrochemical properties, but their task consists of simply reducing crystallization, because no traces of other mechanisms, for example, the specific interaction of Li^+ ions with the particle surface, are found to improve ionic conduction.

Among the types of electrolytes described above, an interesting concept is represented by bicontinuous electrolytes, heterogeneous materials belonging to the class of HEs [16]. HEs are made of two percolating phases, commonly one solid and one liquid. It can be demonstrated through leaching and drying that complete percolation of the liquid phase is achieved, because the specimens after solvent exclusion lose a weight equal to the weight of the solvent present in the wet electrolyte [9, 10, 16, 17]. HEs are typically produced through PIPS, where a polar solvent is mixed with a soluble monomer (or multiple soluble monomers, if copolymers are sought to be obtained) to completely dissolve the resin and get a transparent solution [18]. The percolating liquid phase is sensitive to volatility and leakage unless more viscous solvents are employed. For this purpose, Emilsson *et al.* (2023) studied different linear oligomeric carbonates as solvents for the BMA and obtained ionic conductivity of $2 \cdot 10^{-5}$ S/cm and glass transition temperature (T_g) above 150 °C for an electrolyte containing 40 wt% of solvent [17].

1.2.2. Electrodes

Whittingham, Goodenough, and Yoshino made different contributions to the development of LIBs. Whittingham and Goodenough found a suitable intercalating cathode based on $LiCoO_2$, while Yoshino introduced graphite, another intercalating material, as a replacement for the lithium metal anode [3], to overcome the main limit of this component, that is the formation of dendrites. Nowadays, LIBs are featured by a graphitic anode and an oxide cathode, LFP or $LiMnNiCoO_2$ (NMC), and a scheme can be seen in Figure 1.2a.

The concept of intercalated materials has been applied also to structural batteries, where both electrodes are replaced with carbon fibers (CFs), as illustrated in Figure 1.2b, with the cathode being coated with LFP [19] through electrophoretic deposition [20], to enhance mechanical performance without compromising cycling performance. Cycling consists of alternated cycles of lithiation and delithiation, *i.e.*, the lithium ions insertion and removal from the intercalated anode. CFs are featured by a turbostratic structure, made of graphite sheets, parallel to the fiber axis but folded randomly [6, 21]. Despite their disordered structure, CFs have been proven to show appreciable energy storage capability with respect to graphite, reaching capacities of 250 mAh/g [10], while the maximum theoretical value for graphite is higher but comparable, 372 mAh/g [22]. It was also discovered that low lithiation/delithiation rates improve the capacity to more than 300 mAh/g for intermediate modulus CFs [6], while single fibers rather than bundles prevent the capacity drop after some cycles [6, 23]. CFs can be produced from

mesophase pitch or polyacrylonitrile (PAN), and the precursors determine material strength and stiffness, which ranges between 200-600 GPa of modulus and 3000-6000 MPa of mechanical strength. CFs can have either high stiffness or strength because large and oriented crystals improve stiffness rather than mechanical strength. Between the two types, PAN-based CFs work better as electrodes than pitch-based ones [6, 22]. CFs with large crystals and perfect orientation exhibit a conflict between lithiation effectiveness and stiffness, because they hinder the insertion of ions [6] since they are featured by a graphitic envelopment but a turbostratic core [23], while the accommodation of ions is promoted by amorphous regions instead [23, 24]. Lithiation has minor impact on stiffness and tensile strength after some cycles, while if these properties are analyzed in function of capacity, tensile strength decreases by 5% to 30% according to the type of CFs [6]. During cycling, the first drop in tensile strength is irreversible because a fraction of ions remains entrapped in the structure [24], and it is more intense in fibers with more amorphous regions [23] and in bundles [6], but it is partially restored in the second cycle until it reaches a plateau for further cycles [24].

An alternative to structural batteries where the potential of HEs could be exploited is represented by LMBs (Figure 1.2c). Lithium has a theoretical capacity of 3860 mAh/g, which is one order of magnitude higher than graphite and CFs, but it shows safety issues related to dendrite formation [5]. Dendrites form during lithium plating or cycling and can cause short circuits if they protrude in the LE towards the cathode, but SPEs and HEs can act as physical constraints for anode deposition [17]. Although both electrolytes countervail dendrite growth, it has already been stated that HEs ensure at least one order of magnitude higher ionic conductivity than SPEs.

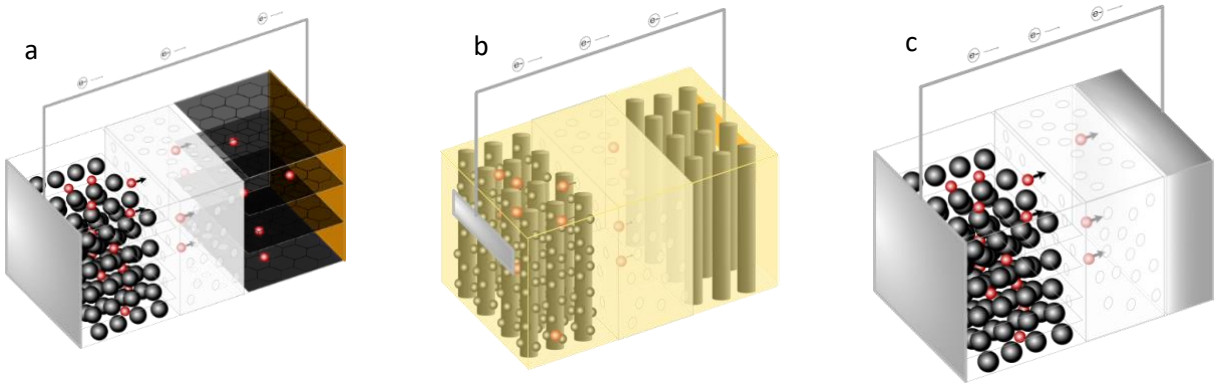

Figure 1.2. Models representing LIBs (a), structural LIBs (b) and LMBs (c). Adapted from [25].

1.2.3. Separator

The separator is responsible for preventing the contact between the electrodes. It must fulfill the same requirements the electrolyte does, with important attention paid to electrical insulating properties. Commercial separators are based on polyolefins *e.g.*, polypropylene (PP), with a microporosity content

of around 40 vol%. Even though PP is proven to work well, some issues must be overcome. Because of its hydrophobicity, PP shows poor wettability towards the electrolyte, hence additional impedance is introduced at the interface. Moreover, thermal shrinkage worsens the adhesion because it further contributes to the detachment from the materials in contact with it. This impedance increase leads to thermal runaway, which is more detrimental for polyolefins because they have low melting temperatures [26]. If the separator lost its shape, the electrodes would risk coming into contact, thus leading to short circuits, followed by uncontrolled development of heat, and the battery could catch fire.

Several attempts aimed to increase thermomechanical stability, for example by introducing aromatic groups, and chemical compatibility, through the introduction of grafted polar groups or ceramic particles, as well as coatings. In doing so, the process becomes more complex and expensive, and the final products are heavier. Crosslinked polymers represent a valid alternative because they provide thermochemical stability. However, this does not mean that the crosslinked polymer is stiff enough to undergo roll-to-roll assembly because weak crosslinks do not provide sufficient stiffness. In copolymers made of polyethylene glycol diacrylate (PEGDA)/1,4-butanediol diacrylate (BDDA), it was found that PEGDA allowed to overcome the threshold of 345 MPa Young's modulus required for roll-to-roll manufacturing [26]. This type of industrial process introduces internal stresses when the strain is released because the separator is constrained by the electrodes that make the sandwich with the separator. Moreover, the formulation was optimized to obtain a separator with high porosity and Young's modulus above 345 MPa and found that adding 63 wt% of ethylene carbonate (EC) to a formulation of PEGDA/BDDA 7/93 wt%, provided 41.3% porosity and $2.09 \cdot 10^{-3}$ S/cm ionic conductivity [26].

1.2.4. Current collectors

LIBs employ metal current collectors because metals are good electrical and thermal conductors, two properties that are sought after for this application [27]. Moreover, they must show a coefficient of thermal expansion (CTE) compatible with the electrodes, otherwise internal stresses would contribute to detaching them from the electrode surface [28]. Aluminum foil is found to work well as a cathode current collector in a wide range of potentials. At high potential, a layer of alumina is formed to prevent corrosion, while, at low potential, the oxide is reduced to metal again. Instead, copper foil is the selected anode current collector because it has good electrical and thermal conductivity and plasticity [27]. One critical aspect that affects the choice of current collectors is the chemical and thermomechanical matching with the electrode, but it can be improved by anodization [28] or the introduction of structured materials [27]. In structural batteries, silver ink is used as an intermediate layer to promote adhesion, and it was demonstrated that screen-printing of the current collector with silver conductive paste led to a less brittle connection than traditional ink application [29].

1.2.5. Interface

The solid electrolyte interphase (SEI) is a 10-50 nm-thick heterogeneous passivation layer of reaction products. It is made of organic compounds like polyolefins and semicarbonates on the electrolyte side and inorganic lithium salts on the side in contact with the electrode [30]. It is important that the SEI is thermodynamically stable, insoluble, and non-porous, and should be flexible enough to withstand the electrolyte volume change. The SEI acts as a filter because it is selective towards lithium ions, while access to solvent molecules is denied [31]. It was discovered that solvent composition and type of electrodes influence SEI quality because carbon-based anodes and prevalence in EC as solvent give better properties [30]. Among these factors, temperature is the most critical aspect because it defines which reactions are thermodynamically favorable. For example, at elevated temperatures, the reaction of EC and lithium ions is favorable. Consequently, more SEI is produced together with ethylene gas, which forms cracks due to volume expansion, and these material discontinuities not only increase internal resistance, but also expose more material for reaction with the electrolyte [31].

1.3. Polymerization-induced phase separation

HEs must exhibit electrochemical and thermomechanical properties compatible with those of the electrodes. Structural LIBs show a trade-off between ionic conductivity and stiffness, since ions flow better in fluids, while only solid materials can keep their shape thanks to strong chemical interactions. One solution to combine both aspects lies in the exploitation of the spinodal decomposition taking place during PIPS. Phase separation can also be induced by a temperature drop (temperature-induced phase separation, TIPS) or an increase in the non-solvent fraction (nonsolvent-induced phase separation, NIPS) [18]. PIPS was first developed for stepwise polymerization of block copolymers [32], but it has been adapted to in-situ free-radical polymerization, where the reagents are a monomer, an initiator, and a solvent. The monomer also takes over the role of the crosslinker, while the solvent, named porogen agent, controls phase separation and pore formation. A scheme of the process is presented in Figure 1.3, where synthesis and curing are sketched.

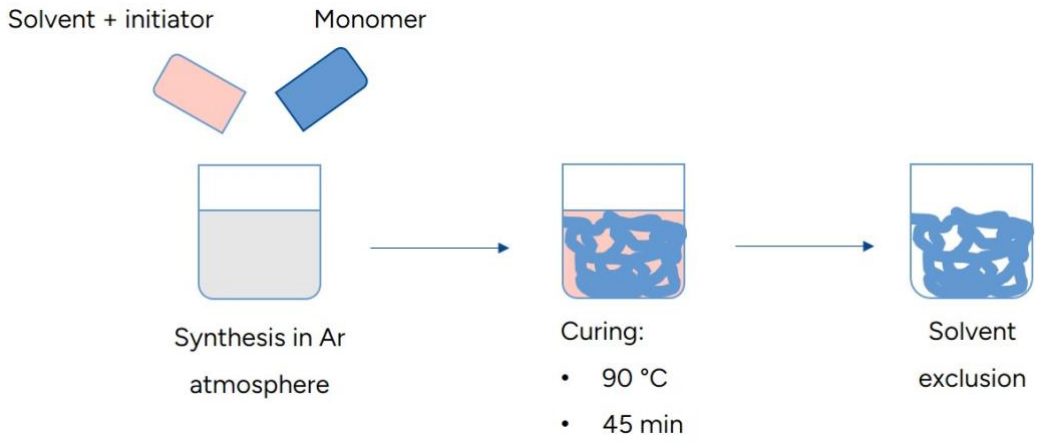

Figure 1.3. Scheme for polymerization-induced phase separation.

PIPS is activated by initiator decomposition through homolytic cleavage, and this suggests that the reaction proceeds through free-radical polymerization. Difunctional monomers are usually employed to get HEs because they promote the formation of a crosslinked network. During network formation, the polymer gradually becomes insoluble in the solvent [6], whereas the monomer molecules remain soluble and can polymerize further in solution [18]. More precisely, in linear polymers, phase separation takes place when the macromolecules become insoluble, while, in crosslinked polymers, the network is formed early, and gelation is reached before phase separation can occur [33]. However, phase separation is observed also in crosslinked polymers. Rather, another mechanism based on the swollen polymer elasticity theory should be considered, which is independent of the parameters described by Flory-Hugging's theory [34]. In this case, the polymer in gel state deswells because of its intrinsic elasticity and releases droplets of solvents, that coalesce together to form the liquid phase. Highly crosslinked polymers undergo early phase separation because of lacking miscibility, but the domains cannot grow much in size. The network is stressed due to crosslinks, and it tends to deswell, causing monomer depletion in the volume around the polymer, thus hindering the addition of further monomers to the polymer and the coalescence of polymer particles [34]. In a few words, the more the polymer is crosslinked, the less accessible it is for reactions with the monomers [35]. Monomers and solvents can be tailored according to the Hansen's solubility parameters to predict phase separation at a certain conversion [9, 17]. HEs promise a Young´s modulus ranging between 360 MPa and 1 GPa and ionic conductivity around 10^{-4} S/cm [6, 9].

BMA is known to perform well as HE, and it is used here as a reference when compared with other monomers. It has been long considered an excellent HE because of its intrinsic stiffness and appreciable crosslinking density when cured, but featured by low viscosity before polymerization [9], due to the presence of the EO groups, which make it suitable for vacuum-infusion. Research aims to find the best compromise between stiff and ionically conductive polymers, provided that the monomers are soluble in the solvent. This combination of properties can be achieved by tuning monomer structure, polymer molecular weight after PIPS, solvent quality and content, fraction of curing agent, and curing temperature [17, 35].

1.3.1. Monomer structure

The inverse relationship between EO length and crosslinking density has already been explored in methacrylates [9]. SEM images revealed smaller pores for monomers having multiple EO units. This result can be explained by considering that EO units make the monomer more polar and, thus more similar to the solvent, which must be intrinsically polar to conduct ions. Therefore, since the limit of solubility is delayed to higher oligomer molecular weights, separation takes place later in the curing stage, when the polymer has already reached low mobility and has become less sensitive to swelling by the solvent. Today, there is a shared opinion that the domain size affects ionic conductivity [36], although previous studies affirmed that it depended only on solvent concentration [9]. The introduction

of EO units in the monomer structure clearly lowers the T_g because crosslinking density, which hinders polymer mobility, is reduced. Moreover, the tan δ peak is narrower and the T_g is well-identified by a clear peak maximum [9].

1.3.2. Type and amount of solvent

A polar solvent promotes the flow of ions along the bicontinuous pathway. EC is highly polar but solid at room temperature, hence it must be mixed with another solvent *e.g.*, propylene carbonate (PC), less polar and less viscous.

Linear carbonates have been analyzed as a replacement for cyclic solvents to improve thermal stability of electrolytes [17]. Low viscosity and volatility cause leakage, but the risk can be reduced by employing solvent molecules with higher molecular weights, which have a higher viscosity. The carbonates studied by Emilsson *et al.* (2023) consisted of the same carbonate unit repeated one, two, or four times (Figure 1.4). It was found out that shorter carbonate oligomers were more compatible with the monomer BMA, hence phase separation was likely to be incomplete at the maximum conversion, resulting in smaller pores, as proved by SEM [17]. This conclusion is consistent with previous statements about the similarity between monomer and solvent [9]. Moreover, using longer carbonates is beneficial for reducing volatility and risk of leakage [17].

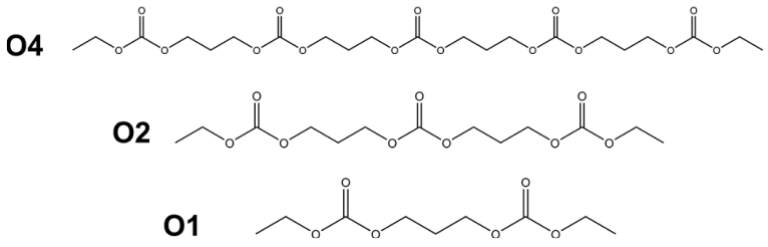

Figure 1.4. Carbonate oligomer structures. Adapted from [17].

As regards the microstructure obtained, it was hypothesized that the interaction between polymer walls and solvent becomes more important for smaller pores, while the tortuosity defined by narrow pores becomes less relevant when the pores are small [37]. This claim can be justified by the increase in ionic conductivity by a factor of seven when the solvent concentration is increased from 40 to 50 wt% [16]. The number of charge carriers is increased linearly with solvent concentration and cannot contribute to enhancing ionic conductivity to that extent. Hence, it must be assumed that morphology, rather than solvent concentration, justifies the unexpected increase in ionic conductivity. Since higher solvent concentrations give origin to larger pores, it can be stated that specific interactions with pore walls are detrimental when little solvent is added, because a larger fraction of solvent falls within the interaction distance of the polymer walls, and it decays according to the third power of the pore diameter.

1.3.3. Temperature

Curing can be conducted through a source of ultraviolet (UV) light or heat. Thermal curing ensures higher conversion and T_g, because the ultimate T_g, which is the transition temperature for fully cured systems, is reached at higher temperatures, especially for densely crosslinked polymers. Recent research stated that curing temperature and technique, thermal or UV-curing, do not affect electrochemical properties [9]. This is not completely true, since UV-curing leads to overall smaller pore size distribution because the initiator is decomposed as soon as it encounters the source, while in thermal curing the initiator molecules cleave gradually while heat diffuses through the sample [10]. Moreover, thermal initiator decomposition should leave voids in the structure [13], but thermal curing is slow, and gases formed can be evacuated outside the structure without affecting the material. On an industrial scale, UV-curing cannot be applied to the cells themselves because CFs are opaque in the UV region and do not allow the radiation to penetrate everywhere homogeneously [10]. A certain amount of reaction heat is released, but CFs can act as heat sinks that absorb heat and prevent the excessive increase in temperature, which is responsible for local thermal degradation [38].

Polymers with an upper critical solution temperature (UCST) become more miscible in the solvent when temperature is increased, and pores are dramatically affected, indeed pore size can be reduced by two orders of magnitude when polymerization temperature is increased from 55 °C to 80 °C [35]. This is one parameter that can be tuned to tailor pore size and get the desired properties, but the size distribution profile may vary also. Temperature indirectly affects solvent-monomer affinity because heat promotes miscibility, while phase separation is delayed since mixing is usually endothermic. Concerning solvent quality, phase separation occurs earlier, and pores are larger in the presence of poor solvent [35]. An increased solubility means that phase separation is delayed to high molecular weights, when few monomers are left unreacted. Proper solvents can solubilize even high molecular-weight polymers, while poor solvents promote polymer precipitation when the molecular weight is still low. Poor solvents help with growth at the same time, because the newly separated polymer domains become more soluble in the monomer than in the solvent, so the monomers concentrate next to the polymer and promote further polymerization, thus contributing to enlarging the domains [35] unless the network is tensed and does not host monomers [34], as discussed in Section 1.3.

Another reason to explain the influence of temperature on morphology is initiator decomposition rate. Since the initiator is sensitive to heat and decomposes at different rates according to curing temperature, it can be stated that, at higher temperatures, a larger number of molecules undergo homolytic cleavage and become free radicals [10]. In that condition, many nucleation spots are formed due to polymer precipitation, while growth is constrained by neighboring polymer globules. Consequently, the resulting structure is characterized by smaller pores [35].

2. Methods

In previous papers, a solvent concentration ranging between 37.5 wt% [9] and 50 wt% [16] was usually chosen. An intermediate solvent concentration of 45 wt% was selected in this context because it represents a good compromise between ionic conductivity and brittleness. Ionic conductivity is related to the number of species that can flow in the liquid phase, hence solvent concentration should in principle be as high as possible. However, it was experienced that above a threshold which depends on the intrinsic polymer flexibility, the material becomes brittle [9], and this issue implies the formation of insulating discontinuities that penalize mechanical resistance and elongation at break.

As regards curing conditions, a temperature of 90 °C was chosen as the best compromise to allow the reaction within a reasonable amount of time while preventing LiTFSI degradation. Previous studies proved that conversion is appreciable at 90 °C.

For a more consistent comparison, three temperatures are considered as references when evaluating the storage modulus curve with respect to temperature. At T=-40 °C all the polymers are in a glassy state, except for BA4. T=25 °C is the temperature corresponding to standard conditions, when the atmospheric pressure is 1 atm, and it can be considered as the average ambient temperature. However, battery applications cover all weather conditions, and a correct performance must be ensured at polar and tropical latitudes. This is the reason why dramatic physical changes in the material are undesired between -30 and 50 °C. Lastly, it is experienced that homoacrylates reach the rubbery plateau, but this is not the case for BMA nor the copolymers, hence an arbitrary temperature of 180 °C, close enough to the upper limit used in DMA analysis, is chosen for a better comparison in tables.

In the present report, the experimental T_g is calculated with respect to the maximum of the tan δ curve. Instead, when the T_g is reported from literature, it is specified how it was calculated. In all figures and tables, the electrolytes are labelled with the notation XXX-E45 (for homopolymers) or XXX-co-YYY-E45 (for copolymers), where XXX and YYY are the names of the monomers. For better readability, the code E45 is implied in the text, unless the fact of not underlining that creates confusion. To the contrary, when pure polymers and dry electrolytes are mentioned, the labels XXX-POL (or XXX-co-YYY-POL) and XXX-DRY (or XXX-co-YYY-DRY) are expressed in graphs, tables, and main text.

Duplicates were collected for samples mentioned in graphs and tables. For EIS analysis, at least three measurements were conducted due to instrument sensitivity. For this reason, standard deviation (STD), whose expression is reported in Equation 2.1, is calculated only for EIS data because it is useful for multiple measurements, where σ_i is the ionic conductivity of the i-sample, σ_{av} is the average ionic conductivity and N is the number of samples analyzed.

$$STD = \sqrt{\frac{\sum_{i=1}^{N}(\sigma_i - \sigma_{av})^2}{N}} \quad (2.1)$$

RT-FTIR analysis was set for 1200 s, but oxygen inhibition and preset time took up some minutes, so the actual reaction was performed for less time, indeed conversion is calculated at 900 s in the following tables, while in graphs, it is reported in the interval between 0 s and 600 s to underline the main changes at the first stage.

2.1. Materials

The electrolyte is made of a polymer belonging to bisphenol A methacrylates or acrylates, a solvent, consisting of EC and PC in a ratio 50/50 vol%, and a lithium salt, lithium trifluoromethanesulphonate (LiTFSI), present in the solvent with a concentration corresponding to 1 M. The reaction was activated by the 2,2'-azoisobutyronitrile (AIBN) initiator.

All chemicals were used as received, without further purification. BMA was obtained from Arkema with 99% purity, while BA1, BA2 and BA4 were purchased from Sigma Aldrich with 99% purity, as well as AIBN, with >98% purity. EC, PC and LiTFSI were purchased from Sigma Aldrich.

The monomers employed here are derived from bisphenol A, that reacted with ethylene oxide first and reacted again with monomers derived from methacrylic acid or acrylic acid *e.g.*, methacrylate and acrylate esters, through a transesterification reaction involving ring opening of the epoxy group. Structure and reaction resemble the synthesis of epoxy resins, commonly used as matrices for FRPs. Epoxy resins belong to the class of vinyl esters, which differ from bisphenol A ethoxylates because they have a pending hydroxyl group. The difference in the chemical structure depends on the reagents used, epichlorohydrin for vinyl esters and ethylene oxide for bisphenol A ethoxylates.

The formulation composition is summarized in Table 2.1, while the variety of monomers used is illustrated in Figure 2.1 and the chemical structures of EC, PC and LiTFSI in Figure 2.2. In 0.818 g solvent there were 0.352 g EC, 0.320 g PC and 0.146 g LiTFSI, considering EC and PC having densities of ϱ=1.32 g/cm^3 and ϱ=1.20 g/cm^3 respectively and LiTFSI molar weight M_w=273 g/mol.

Table 2.1. Reagents and relative amounts requested for each formulation. The label *solvent* stands for EC/PC 50/50 vol% containing 1 M LiTFSI.

Name	Methacrylate (g)	Acrylate (g)	Initiator (g)	Solvent (g)
BMA	0.990	0	0.010	0.818
BA1	0	0.990	0.010	0.818
BA2	0	0.990	0.010	0.818
BA4	0	0.990	0.010	0.818
BMA-co-BA1	0.495	0.495	0.010	0.818
BMA-co-BA2	0.495	0.495	0.010	0.818
BMA-co-BA4	0.495	0.495	0.010	0.818

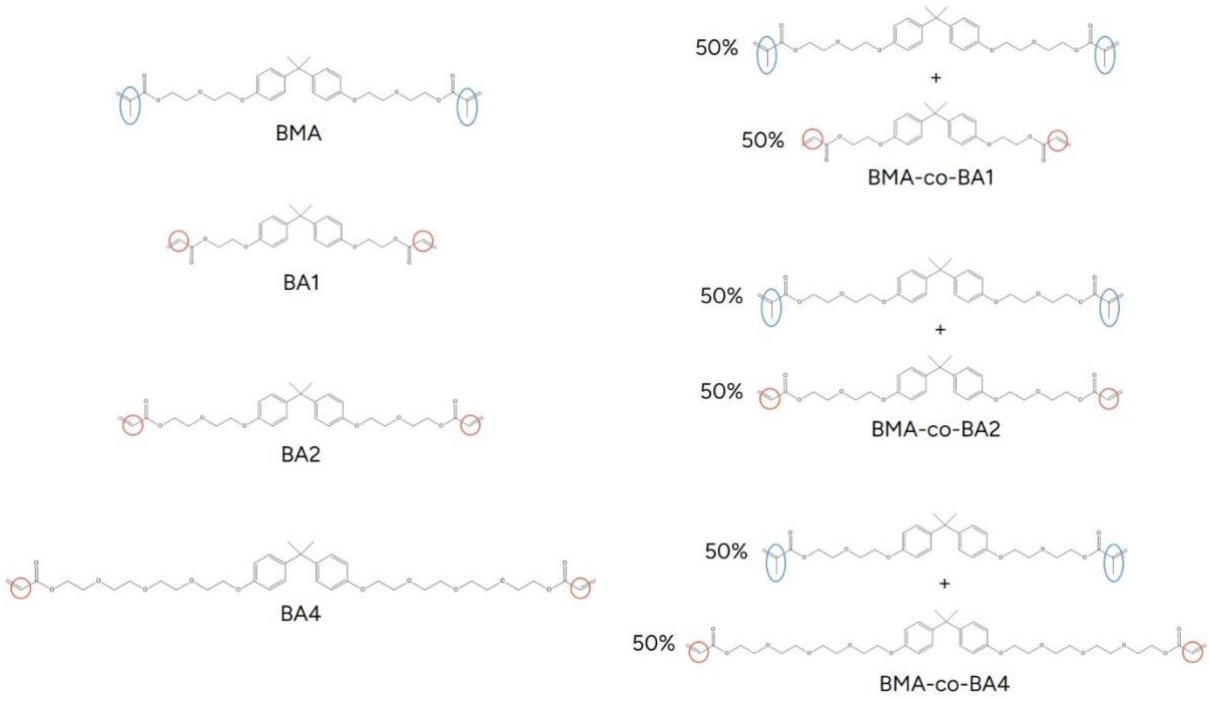

Figure 2.1. Monomer structures representing all the HEs synthesized.

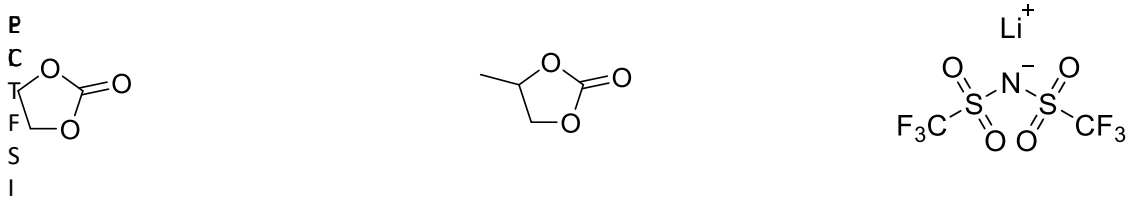

Figure 2.2. Solvent and lithium salt structures.

2.2. Experimental

2.2.1. Synthesis

Electrochemical cells are affected by moisture and oxygen present in the atmosphere, and this is the reason for producing them in a closed chamber in inert atmosphere, where oxygen and moisture levels are kept below 1 ppm. The connection with the inner side of the chamber is possible through thick rubber gloves and a polycarbonate panel (Figure 2.3).

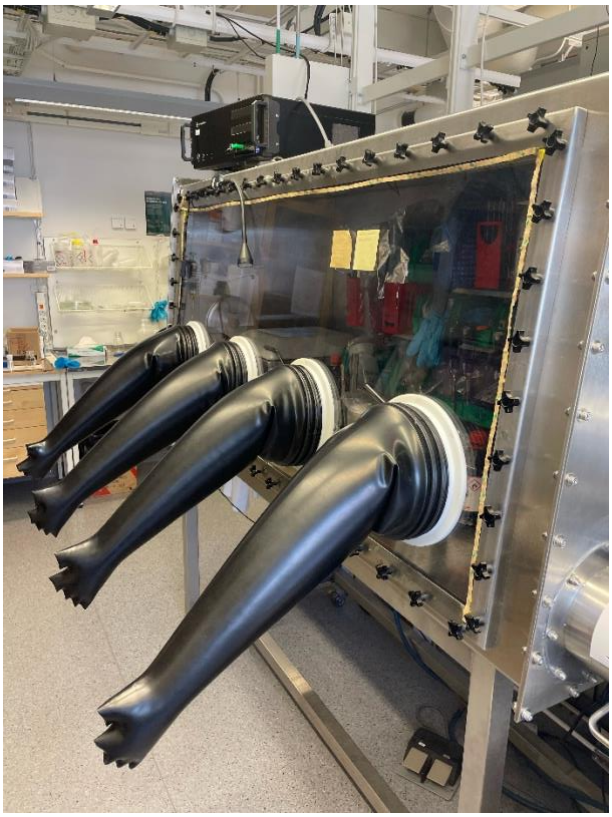

Figure 2.3. Glovebox for the synthesis in a protected atmosphere.

EC is solid at room temperature, and it must be heated at 60 °C to promote melting. EC and PC were mixed according to the 50/50 vol% ratio. The mixture was injected into the vial where LiTFSI had been weighed, and dissolution was promoted by a vortex machine. Then, the solution of solvent and salt was injected into the vial containing the right amount of AIBN and homogenized again. A stock solution was prepared to synthesize multiple electrolytes in parallel. After that, the monomers were weighed and the correct amount of solvent plus AIBN was injected into the vial to respect the 55/45 wt% ratio. The formulation was mixed with the aid of the vortex machine, then injected onto aluminum molds sized 30x5x0.5 mm. A glass slide was applied on top and clamped with the mold at the edges. The system was enveloped in an aluminum bag with a sealing machine and brought out of the glovebox for curing.

Curing was conducted at 90 °C in oven for 45 minutes. Before removing the samples from the mold, the bag was brought inside the glovebox again to perform EIS.

Pure polymers, instead, were synthesized in a fume hood in ambient atmosphere because oxygen and moisture are not critical for them. Since AIBN is not soluble in the monomers, an auxiliary solvent was used. Acetone was chosen first, but n-butyl acetate was preferred later to overcome bubble formation in the final polymer. Polymers containing defects were hard to test through DMA because they fractured in weak points. Since the solvent affects thermomechanical properties, only a few droplets were introduced into the vial containing the monomer and let evaporate for an hour. It was important to let the solvent evaporate before filling the molds, otherwise it remained entrapped between the mold and the slide.

Dry polymers were tested through DMA after electrolyte leaching for 24 h and vacuum drying for the same amount of time. Samples used for solvent exclusions were suitable for this purpose.

2.2.2. Electrochemical impedance spectroscopy

EIS analysis was performed using the Gamry Series G 750 Potentiostat/Galvanostat/Zero Resistance Amperometry (ZRA) interface connected to a four-point resistance setup, with golden working electrodes at a distance or 5 mm and reference electrodes at 20 mm (Figure 2.4). The setup was used in the potentiostatic mode, where small-amplitude voltage impulses in the order of mV in a broad range of frequencies were created and the respective current was measured.

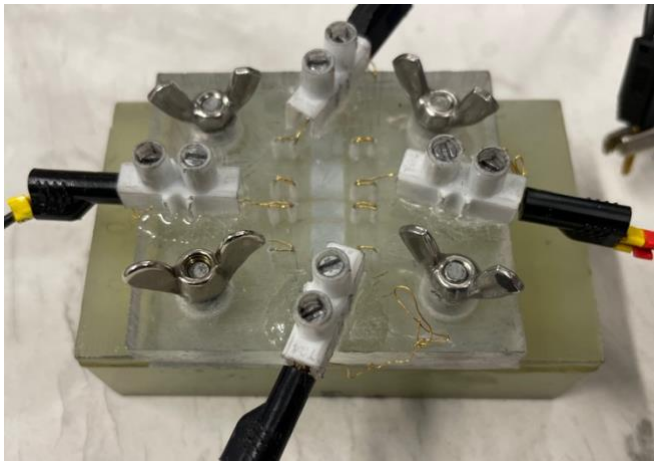

Figure 2.4. Setup for the EIS analysis.

Voltage and current are represented by sinusoidal functions dependent on frequency. The software calculated the impedance, given by the ratio between voltage and current, according to the first Ohm's law (Equation 2). The current is out of phase with respect to the voltage and this means that the impedance has two components, one real and one imaginary. In Equation 2.2, Z is the impedance,

characterized by the real value Z_{real} and the imaginary value Z_{imag}, $\psi(\omega)$ and $j(\omega)$ are the voltage and current respectively, that are function of the frequency, denoted by ω, while φ measures how much the current is out of phase with respect to the voltage.

$$Z(\omega) = \frac{\psi(\omega)}{j(\omega)} = \frac{\psi \cdot sin\, \omega t}{j \cdot sin(\omega t + \varphi)} = Z_{real} + iZ_{imag} \quad (2.2)$$

The phenomena responsible for the conduction have different time constants [39]. The electrical conductivity is calculated as in Equation 2.3, where σ is the conductivity (in S/cm), e=1.6·10^{-19} C is the elementary charge, n the number of charges moved per unit volume (in C/cm^3) and μ is the electron mobility (in cm^2/(V·s)). Electron mobility depends on the lattice structure in which the charge carriers must flow, on temperature, but also on the effective mass of charge carriers [40], and this explains why different time constants can be identified for different charged species.

$$\sigma = e \cdot n \cdot \mu \quad (2.3)$$

Impedance is visualized on a graph called Nyquist plot, where Z_{real} and the opposite of Z_{imag} are represented on the x-axis and y-axis, respectively. The figure drawn is a semicircle that crosses the x-axis in two points. The intercept with the x-axis on the left side, corresponding to high frequencies, represents the electrode resistance, while the right point is referred to the bulk electrolyte resistance plus the internal electrode resistance [39, 41]. An example of Nyquist plot is represented in Figure 2.5a, where the semicircle has already been shifted, so that the left interception corresponds to the origin of the axes and the electrode internal resistance is neglected. In Figure 2.5b, the resistance, corresponding to Z_{real}, is represented with respect to the frequency. Resistance reaches a plateau at low frequencies. It is convenient to underline that the graphs in Figure 2.5a-b, valid for BMA as an example, represent the same result in two different ways.

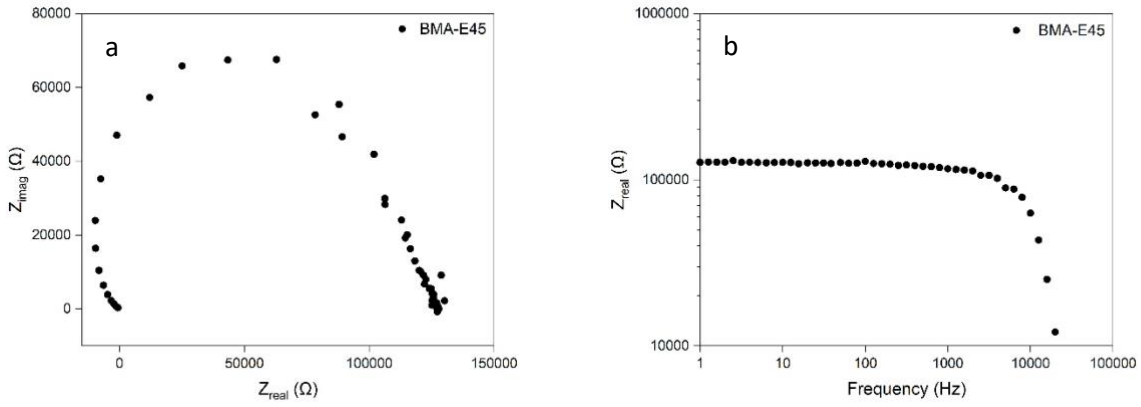

Figure 2.5. Nyquist plot (a) and real component of the impedance with respect to the frequency (b) for BMA-E45.

To summarize, the semicircle diameter estimates the bulk electrolyte resistance, the value used to calculate ionic conductivity. Once the resistance is given, ionic conductivity can be calculated from geometric parameters through second Ohm's law, as specified in Equation 2.4, where σ is the ionic conductivity, l=5 mm the distance between the electrodes, A the cross-sectional area and R_Ω the resistance measured by the instrument. Width and thickness of the samples tested were measured by a digital slide caliper and a thickness gauge, respectively.

$$\sigma = \frac{l}{A \cdot R_\Omega} \tag{2.4}$$

2.2.3. Fourier-transform infrared spectroscopy

FTIR analysis was performed using the PerkinElmer Spectrum 100 FTIR Spectrometer equipped with the Specac Golden Gate Diamond attenuated total reflectance (ATR) accessory and a deuterated triglycine sulfate detector. The instrument was connected to the PerkinElmer Spectrum software. The spectrometer is illustrated in Figure 2.6a, while the detail of the ATR accessory is highlighted in Figure 2.6b. Eight scans per sample were integrated in one spectrum in the range between 600 and 4000 cm^{-1} with a resolution of 4 cm^{-1}. For each type of electrolyte, both the resin and the cured polymer were analyzed. The resin was analyzed within a few hours after mixing, because AIBN decomposes also at room temperature, even if at low rates, but the measurement could be triggered if the FTIR analysis were conducted after longer time.

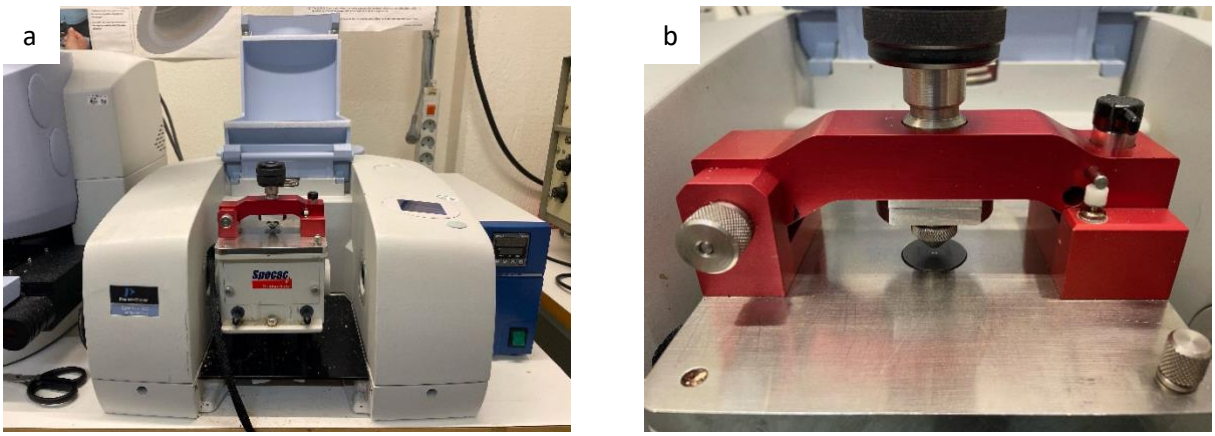

Figure 2.6. PelkinElmer Spectrometer (a) equipped with the Specac Golden Gate Diamond ATR (b).

FTIR analysis is useful to investigate vibrational energies of chemical bonds because they have transition energies in the order of the infrared radiation (IR), included in the region between 2.5 and 25 μm. FTIR spectra are graphs representing the absorbance or transmittance with respect to the wavenumber, that is defined as $1/\lambda$, with λ the wavelength, and it is expressed in cm^{-1}. One typical spectrum for BMA-co-BA1 as an example is visualized in Figure 2.7 in the range 600-4000 cm^{-1}.

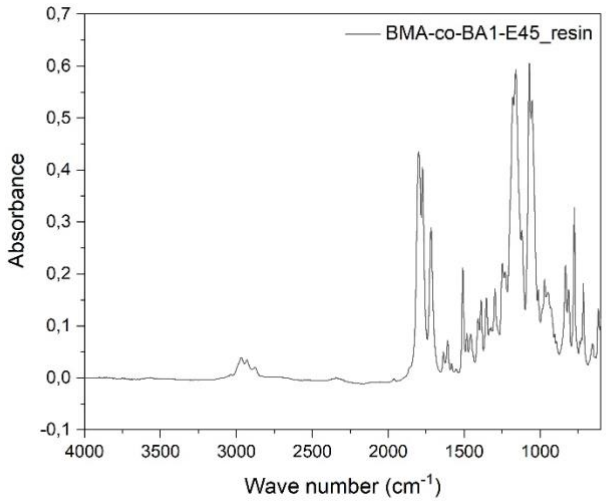

Figure 2.7. FTIR spectrum for BMA-co-BA1-E45 resin.

The carbonyl peak could be chosen as internal reference because it does not intervene in the reaction. However, curing reduces its absorbance, indeed the area of the vinyl peak should be related to the area underneath the carbonyl peak rather than its maximum height. Due to the presence of solvent, the carbonyl peak partially overlaps with the carbonate peaks at around 1800 cm^{-1}, and it would be difficult to distinguish the two contributions. For this reason, it is simply chosen to set the interactive baseline correction at 4000 cm^{-1} and 2000 cm^{-1}. In doing so, the conversion is only slightly underestimated.

2.2.4. Real time Fourier-transform infrared spectroscopy

Unlike FTIR, the plate is heated to 90 °C to simulate the curing process in the oven. Since the resin has been in contact with the atmosphere, at a first stage the reaction is hindered because of oxygen inhibition, otherwise no other effects of the atmosphere on the reaction are reported. Therefore, conversion is simply evaluated after the oxygen inhibition stage has ended.

Thin films are expected to polymerize faster than massive samples for two reasons. First, the initiation step is postponed in the bulk in comparison with the surface, when heat is conveyed through a heat insulating material, due to low thermal diffusivity. Moreover, the thermal diffusivity of air is lower than that of solids, hence it requires time for the samples in the oven to increase their temperature with respect to the resin in direct contact with the heat source.

The conversion rate was studied through real-time FTIR to evaluate the time taken for the system to reach a certain conversion. For simplicity, 80% and 90% conversions have been considered arbitrarily, and the times are reported after the oxygen inhibition step is completed, with no further corrections necessary.

2.2.5. Dynamic mechanical analysis

DMA analysis was performed using the DMA Q800 V21.3 Build 96 instrument equipped with a liquid nitrogen cooling accessory and connected to the TA Instrument Explorer software. Data were analyzed through TA Universal analysis software.

The experimental part was carried out in tensile film mode through a temperature ramp frequency sweep test. A preload force of 0.125 N was applied, while the amplitude strain was set at 0.1% and the frequency at 1 Hz. The temperature ramp was set at 3 °C/min heating from -50 °C to 150 °C for acrylates and 200 °C for BMA and copolymers. Before the experiment started, an initial stage of stabilization at -50 °C for 5 minutes was included. Samples were mounted on clamps at a 10-15 mm distance. The setup is illustrated in Figure 2.8.

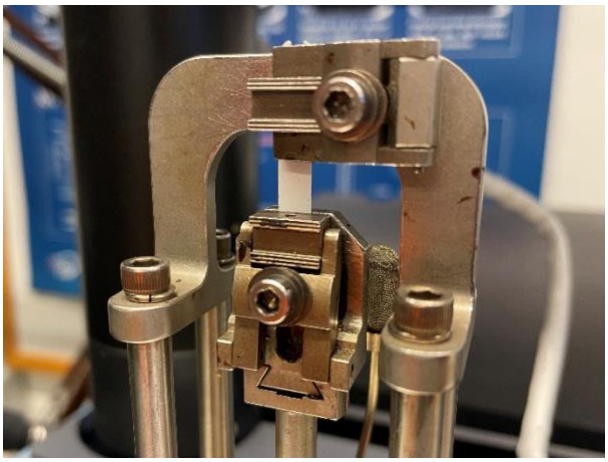

Figure 2.8. Sample installation on the DMA instrument.

Polymers are viscoelastic materials that can be modeled through a spring and a dashpot, which represent the elastic and viscous contributions, respectively. The spring is governed by Hooke's law in Equation 2.5, while the dashpot by Newton's law in Equation 2.6.

$$\sigma = E \cdot \varepsilon \tag{2.5}$$

$$\tau = \eta \cdot \frac{\mathrm{d}\varepsilon}{\mathrm{d}t} \tag{2.6}$$

As can be seen, there is a direct relationship between stress and strain in ideal elastic materials, while stress is related to the first derivative of strain with respect to time in viscous fluids. When a sinusoidal strain is applied, as defined in Equation 2.7, the material response is instantaneous in elastic materials and delayed in time in viscous materials. This means that the measured stress is in phase with the applied strain in pure elastic materials, while it is delayed by $\pi/2\omega$ in pure viscous fluids (Equations 2.8-2.9). Viscoelastic materials are intermediate between these boundaries, and the phase delay depends on the ratio between the viscous and elastic contribution.

$$\varepsilon(t) = \varepsilon \cdot \sin \omega t \tag{2.7}$$

$$\sigma(t) = E \cdot \varepsilon \sin \omega t \tag{2.8}$$

$$\tau(t) = \eta \cdot \varepsilon \cdot \omega \cos \omega t \tag{2.9}$$

DMA technique can set apart the two components into storage modulus (*E'*) and loss modulus (*E''*), and another physical variable, named tan δ, is derived from the ratio in Equation 2.10.

$$\tan \delta = \frac{E''}{E'} \tag{2.10}$$

DMA is a sophisticated technique to measure the T_g of polymers, where DSC often cannot underline that [42]. The curve described by tan δ can be used to determine the T_g of polymers because a peak can be detected, corresponding to the situation where the loss modulus prevails over the storage modulus. Indeed, T_g is defined as the temperature at which the macromolecules are mobile enough to activate cooperative movements and disentangle, and on a macroscopic scale, it can be detected through an increase in material flexibility.

The storage modulus in the plateau region for thermoset materials gives information about crosslinking density, indeed the storage modulus and the molecular weight of spacers between crosslinks are related through an inverse law, as expressed in Equation 2.11 [43], where M_c represents the molecular weight between chemical joints, ρ the bulk density, R the universal gas constant, T the absolute temperature and E' the storage modulus in the plateau region. This is valid under the assumption of having a pure polymer, but it is not true for electrolytes, because the solvent is a softener and crosslinking does not occur in the liquid phase.

$$M_c = \frac{3 \cdot \rho \cdot \mathrm{R} \cdot T}{E'} \tag{2.11}$$

2.2.6. Physical observation

Opaqueness can provide an initial idea about the size of the phases present in the material, because pores and defects in general, are able to scatter the light when the size of the obstacle and the radiation wavelength are comparable (λ=380-760 nm for visible light). To summarize, larger pores are in general associated with a wider range of scattered radiation, which is the radiation with a wavelength smaller than the pore size. Opaqueness evaluation is not conclusive unless it is corroborated by SEM micrographs. Even though SEM is a qualitative technique, it is useful to highlight morphology and distinguishing different microstructures.

2.2.7. Scanning electron microscopy

SEM observation was conducted using a Hitachi S-4800 microscope equipped with a cold field-emission electron source. SEM microscopes operate under vacuum, and for this reason, it is important that only dry samples are introduced in the chamber. Samples used for solvent exclusion, for example, are suitable because they have been soaked in deionized water for 24 h to leach the solvent out and then vacuum

dried at 50 °C for another other 24 hours to remove water molecules that might have been entrapped in the pores.

Specimens were cryo-fractured with the aid of liquid nitrogen. At T=-196 °C, even the softest polymers are in the glassy state, allowing for a brittle fracture. Carbon (or copper) tape was applied to the SEM stub and the fragments were attached to the tape, with the cross-section facing upwards. After the fragments were attached to the tape, the SEM stub appeared as shown in Figure 2.9. Then, a 2 nm-thick platinum-palladium coating was applied through sputtering by a Cressington 208HR sputter coater, with a 40-mA current applied for 15 s.

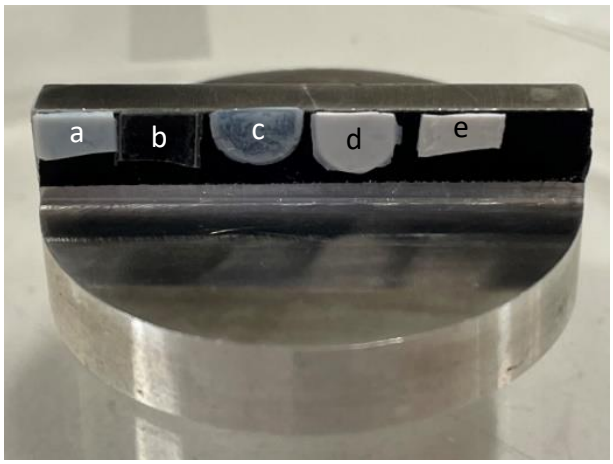

Figure 2.9. SEM stub with the cryo-fractured samples aligned, a) BMA-E45, b) BA2-E45, c) BA1-E45, d) BMA-co-BA2-E45 and e) BMA-co-BA1-E45.

SEM can be used to evaluate the surface topology and morphology of samples through two different types of electrons detected. Back-scattered electrons (BSE) give information about the phases present on the surface, and they are useful if the phases are made of atoms with different atomic masses. In contrast, secondary electrons (SE) provide information about the surface morphology and highlight hills and valleys. Only SE are relevant in the present research because surface roughness is more relevant here, while the composition does not differ between the polymer phase and the solvent, as they are both made of compounds containing carbon, oxygen, and hydrogen.

2.2.8. Solvent exclusion

Samples for solvent exclusion were dried for 24 hours in a vacuum oven at 50 °C, after soaking in excess deionized water for 24 hours. They were weighed within one day after synthesis and immediately after drying.

3. Comparison of methacrylates and acrylates

Monomers polymerizing through PIPS must contain functional groups with heteroatoms in their structure, which promote solubility in polar organic solvents. Moreover, if they are requested to be suitable for structural batteries, they must integrate functional groups that hinder macromolecule mobility *e.g.*, aromatic rings, and side chains. As regards the solvent, it must be compatible with the electrodes and form a stable SEI, and provide coordination with the ions, Li^+ and $TFSI^-$. It must be underlined that the electrolyte is designed to provide ionic conduction, but not electronic conduction because the electrons must be conveyed to the external circuit through current collectors, while ions are exchanged between the anode and the cathode through electrolyte and separator. Monomers with polar functional groups and without conjugated double bonds are the best candidates for this purpose.

BMA has been widely studied as a suitable HE for LIBs. HEs are commonly obtained through PIPS, where two bicontinuous phases percolate the material [32]. Ionic conductivity of BMA samples in inert argon atmosphere with an electrolyte concentration of 40, 45 and 50 wt% was calculated to be around 10^{-4} S/cm [16]. These outcomes are considered promising because, even if BMA is one order of magnitude less conductive than GPEs and two orders less than LEs, it has overall higher mechanical properties. These are demonstrated through DMA analysis, which shows a storage modulus of 550 MPa at room temperature (T=25 °C), as illustrated in Figure 3.1, similar to previous results obtained under the same curing conditions [10]. UV-curing on the same monomer led to a storage modulus of 360 MPa, around 25% lower [9]. This difference is due to UV-curing, which leaves around 15% unreacted vinyl groups [10]. Unsaturations are detrimental for electrolyte degradation, and they limit the expression of mechanical performance of the polymer phase. Moreover, as presented in paragraph 1.3.4, UV-curing is associated with smaller pores and lower ionic conductivity, even though some researchers stated that there is no experimental evidence that the technique affects electrochemical performance [10]. As regards the present work, the T_g cannot be detected clearly because the peak is beyond the temperature range selected for testing, but it is clearly above 170 °C. Broad peak also indicates that the polymer is highly crosslinked.

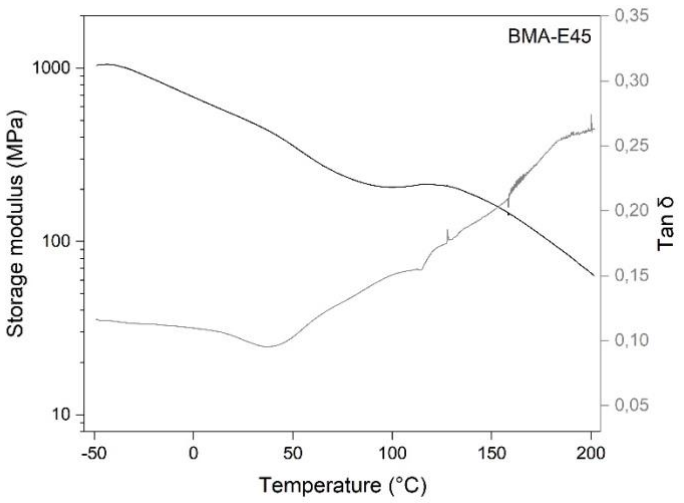

Figure 3.1. DMA analysis for BMA-E45.

3.1. Polymerization

From the literature, acrylates are known to polymerize faster than methacrylates [44, 45]. Table 3.1 shows that the polymerization rate, expressed by the polymerization kinetic constant $(k_p/k_t)^{1/2}$, where k_p and k_t are the propagation and termination rate constants respectively, is ten times higher in n-butyl acrylate than in n-butyl methacrylate [46]. This behavior may be related to chain mobility at the curing temperature, which is connected to chemical structure. Moreover, a secondary carbon radical is formed in acrylates, which is more unstable than the tertiary radical in methacrylates [47]. A free radical is an atom with an unpaired electron, that has been lost because of homolytic cleavage. In tertiary carbon radicals, typical of methacrylates, the methyl groups partially counterbalance the missing negative charge through their inductive effect, thus making the radical more stable and less reactive. More specifically, methyl groups tend to move their electron cloud towards electron-deficient species and share the charge. The inductive effect is gradually reduced in secondary, primary and methyl radicals.

Table 3.1. Homopolymerization rates for n-butyl methacrylate and n-butyl acrylate at 80 °C. Data obtained from [46].

Monomer	**K_p** **(L mol^{-1} s^{-1})**	**K_t** **(L mol^{-1} s^{-1})**	**$(K_p/K_t)^{1/2}$** **(L$^{1/2}$ mol$^{-1/2}$ s$^{-1/2}$)**
N-butyl methacrylate	1.22×10^3	1.44×10^7	0.32
N-butyl acrylate	4.97×10^4	1.99×10^8	3.53

During polymerization, acrylates undergo autoacceleration, which leads to the formation of gel points [48]. This phenomenon is also named after Trommsdorff-Norrish, who first studied it. Autoacceleration takes place under isothermal conditions and can be explained by referring to the quick increase in viscosity caused by the growing polymer, which hinders the translational diffusion *i.e.*, the movement of two oligomer radicals towards each other [49]. Hence, the probability that two radicals come close enough with each other to react decreases. At the same time, however, the reactivity of radicals does not change with viscosity and propagation goes on until an even more viscous medium is obtained.

The difference in termination rates in Table 3.1 can be explained by the different termination mechanisms taking place for methacrylates and acrylates, that can be either combination or disproportionation, but they both intervene simultaneously in real systems. In combination, two oligomeric radicals react and form a single macromolecule, whose molecular weight is the sum of the molecular weight of the combined macromolecules. In disproportionation, instead, one hydrogen belonging to the methyl group bound to the radical is torn away from one macromolecule, so that an unsaturation is formed in one of the macromolecules, while the other has gained one hydrogen and established the neutrality again [50]. The competition between combination and disproportionation is governed by the number of hydrogens available for being torn away, radical reactivity, already mentioned in the previous paragraph, and steric hindrance of substituents bound to the radical, with the reactivity being less relevant than the other contributions [51]. Moreover, methacrylates can react either by combination or disproportionation according to the alkyl chain length, indeed cumbersome alkyl groups make disproportionation more likely to happen than combination, but they are also dependent on the temperature because at high polymerization temperatures methacrylates react preferably through disproportionation [50]. Since BMA has a bulky ester group, it can be stated with good approximation that disproportionation is the dominating mechanism here. On the other side, there is widespread agreement with the fact that acrylates react through combination, even though previous studies, which were tricked by transfer reactions, claimed the opposite [50].

High conversions are important not to leave unsaturations that may give unexpected reactions [9]. Thermal curing is usually chosen for high T_g polymers to avoid early vitrification [17, 38], which is known to be responsible for incomplete reaction because it leaves radicals trapped in the glassy polymer [44, 52]. Moreover, it was demonstrated that thermal curing allowed to obtain slightly higher mechanical properties, even though it can cause initiator decomposition to form gases that remain entrapped in the structure [13], but AIBN is present at such low concentrations that it has a negligible impact if any.

It was decided to follow up previous research by studying one methacrylate and one acrylate in parallel, both derived from bisphenol A ethoxylate, to accomplish the requirements of polarity and internal stiffness. The methacrylate chosen for this purpose is BMA, which structure is represented in Figure 3.2, together with the respective acrylate, BA2. The reason for choosing a solvent concentration of 45 wt% has been discussed in Chapter 2.

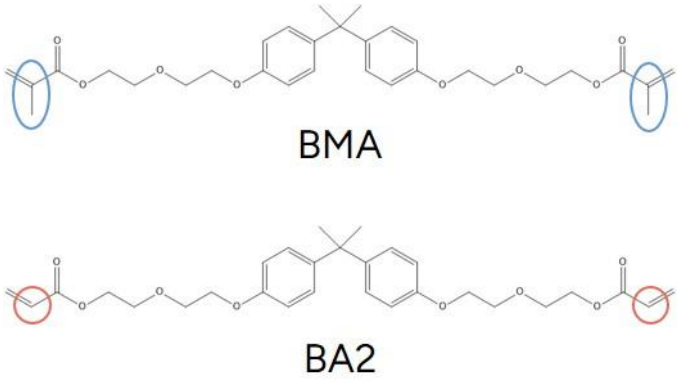

Figure 3.2. Monomer structures representing BMA and BA2.

BA2 shows higher conversion than BMA, both as electrolyte and pure polymer, as demonstrated by the conversion extrapolated from the RT-FTIR analysis (Figure 3.3). It is obvious that the electrolyte has faster conversion because the solvent acts as a plasticizer and promotes chain mobility. Table 3.2 shows how much time the monomers take to reach 80% and 90% conversion and the conversion after 15 minutes. This data agrees with the FTIR analysis on samples cured at 90 °C for 45 minutes. A comparison is offered in Table S1 in the Supporting Information.

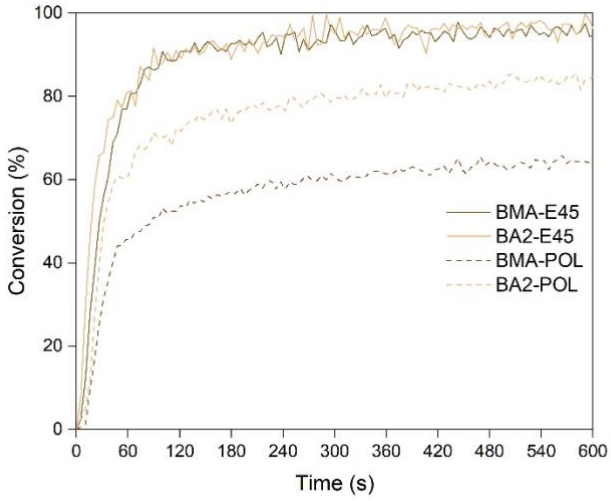

Figure 3.3. Conversion obtained from RT-FTIR analysis for BMA-E45, BMA-POL, BA2-E45 and BA2-POL.

Table 3.2. Data extrapolated from RT-FTIR analysis.

Polymer	**$t_{80\%}$ (s)**	**$t_{90\%}$ (s)**	**Conversion$_{\|t=15\ min}$ (%)**
BMA-E45	60	120	97
BA2-E45	60	120	97
BMA-POL	>1000	>1000	68
BA2-POL	330	>1000	87

3.2. Thermomechanical properties

Methacrylates and acrylates have been compared in previous studies [46, 53], with the aim to investigate the effect of the addition of a methyl group in the structure on thermomechanical properties.

In general, it can be said that methacrylates are rigid and have high T_g, because the methyl group contributes to the formation of entanglements. Regardless of the chemical structure, it seems that methacrylates exhibit around 80 °C higher T_g than the respective acrylates, at least for the most common polymers, as underlined in Table 3.3. T_gs reported from Hughes *et al.* (1961) and Krause *et al.* (1965) were measured at the onset of the storage modulus drop [54, 55]. Friedrichs *et al.* (2013) measured the T_g through DSC [56]. Rehberg *et al.* (1944) measured the brittle point through flexing upon immersion in ethanol cooled with solid carbon dioxide [57]. Shetter (1963) measured the gel melting point as the temperature above which a gel inserted into a pipet flows out of a standardized needle [58].

Table 3.3. Literature T_g values for methacrylates and acrylates.

Alkyl chain	**Poly(methacrylate)**	**Poly(acrylate)**
Methyl	$T_{g,(PMMA)}$=105 °C [54]	$T_{g,(PMA)}$=8 °C [54]
Ethyl	$T_{g,(PEMA)}$=67 °C [56]	$T_{g,(PEA)}$=-22 °C [54]
Iso-propyl	$T_{g,(PPMA)}$=78 °C [55]	$T_{g,(PPA)}$=-8 °C [55]
N-butyl	$T_{g,(PBMA)}$=19 °C [54]	$T_{g,(PBA)}$=-54 °C [54]
Iso-butyl	$T_{g,(PBMA)}$=48 °C [55]	$T_{g,(PBA)}$=-24 °C [57]
Ter-butyl	$T_{g,(PBMA)}$=107 °C [55]	$T_{g,(PBA)}$=43 °C [58]

Experimental results on BMA and BA2 show that the difference in T_g between BMA and BA2 is far higher than 80 °C, indeed BA2 exhibits a clear Tan δ peak at 14 °C, while it is well above 170 °C for BMA (Figure 3.4a). Moreover, since the tan δ values are related to a variation in the slope of the storage

modulus with temperature, it means that stiffness drops more quickly in BA2, and this is confirmed by DMA results shown in Figure 3.4b. Consequently, the transition is completed in a tight temperature interval. This is not necessarily a drawback, unless the properties are constant in the temperature range where the HE is supposed to work.

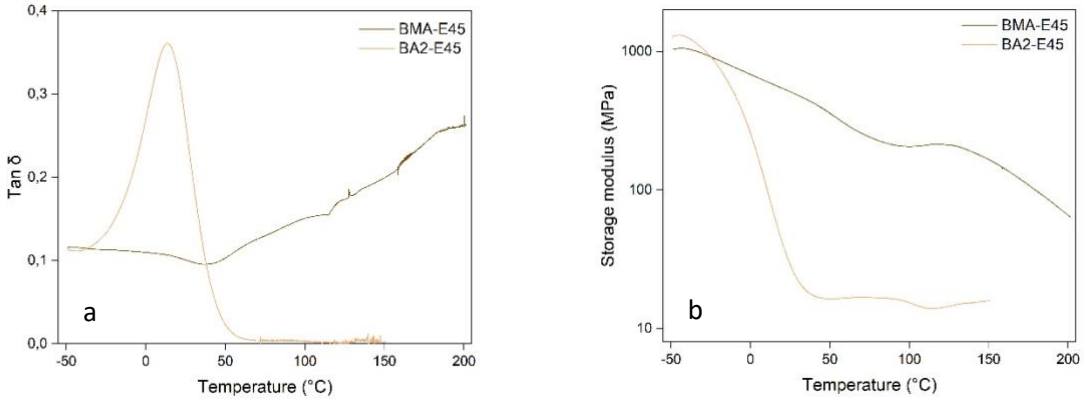

Figure 3.4. Tan δ peak (a) and storage modulus (b) for BMA-E45 and BA2-E45.

As expected, the storage modulus of BA2 is 95% lower than BMA already at 25 °C, even though in the glassy state they have comparable stiffness. This represents a limit of application for BA2 if it would be used in structural batteries, but it could rather be an opportunity for other types of energy storage devices *e.g.*, flexible batteries [6]. However, a physical transition is undesired at the working temperature. Therefore, if BA2 were considered suitable as electrolyte, its T_g should be pushed towards lower temperatures, so that it would be possible to work completely in the rubbery range. It is important to underline that BA2 would be feasible as hybrid electrolyte if it had higher or comparable ionic conductivity as BMA, but this aspect is investigated in Section 3.4.

For completeness, in Figure S1 in the Supporting Information, the pure polymer BA2-POL is compared with the respective electrolyte BA2-E45. As expected, the transition temperature is delayed at higher temperatures, 54 °C against 14 °C (Figure S1a), because the plasticizing effect of the liquid solvent is missing. Moreover, the storage modulus is higher in the whole interval (Figure S1b) and the difference is remarkable at higher temperatures because the bulk polymer is less sensitive to temperature increase than the electrolyte for the same reason.

The idea of moving towards less stiff electrolytes even for structural batteries is reasonable because a certain degree of flexibility is requested for the electrodes to accommodate ions more easily in their intercalated structure [59] and not to fracture after several cycles where the internal pressure is increased and decreased repeatedly [60]. Though, such a large drop with respect to the state-of-the-art HEs risks being detrimental rather than effective. According to Willgert *et al.* (2011), who tested formulations of

two monomers in different concentrations, even the stiffest polymers with E'=1200 MPa at room temperature provided at least 10% elongation at break [13]. However, they dealt with SBEs, whose ionic conductivity depended on the structure flexibility and no bicontinuous structures were foreseen. The presence of discontinuities in the material is likely to lead to a softer and more brittle material at the same time.

In Table 3.4, the difference between the porous structure and the pure bulk polymer can be observed. In the glassy state, it is expected that the electrolyte is around 45% less stiff than the pure polymer, because the solvent is a liquid, and its stiffness can be assumed to be zero. The deviation is remarkable for BMA, since BMA-E45 is 70% less stiff than BMA-POL, while it is aligned with the prediction for BA2-E45, that is around 50% less stiff than BA2-POL. This deviation could be ascribed to a non-homogeneous pore distribution because the mechanical properties may be limited by the region of the specimen where the pores are more concentrated, and the polymer is less dense in turn. Another reliable reason could be the presence of solvent in the polymer phase, which softens the crosslinked network more than it would do if it were completely confined in the liquid phase [9]. This hypothesis is supported by Cattaruzza *et al.* (2023), who demonstrated through gravimetric swelling that a fraction of solvent (8-10%) is found inside the polymer phase [16], and Emilsson *et al.* (2023), who calculated the volumetric shrinkage after drying to be 20-30% according to the type of linear carbonate used as solvent [17]. In addition, the solvent is absorbed by the polymer while the lithium salt preferably remains in the porous phase, indeed its concentration in the polymer is 0.2-0.3 M, lower than in the initial formulation [16]. Such a small amount of absorbed solvent is not enough to classify the polymer as a GPE, because most of it is present in the bicontinuous porous phase, but it may have an impact on the thermomechanical properties anyway. Manly and Tenhaeff (2022) produced the same conclusions, even if they studied porous separators, rather than electrolytes, based on PEGDA/BDDA copolymers [26].

Table 3.4. Storage modulus at different temperatures for BMA-E45 and BA2-E45.

Polymer	**$E'_{glassy\ (T=-40\ °C)}$ (MPa)**	**$E'_{\|T=25\ °C}$ (MPa)**	**$E'_{rubbery/180\ °C}$ (MPa)**
BMA-E45	1100	550	~200
BA2-E45	1200	30	~20
BMA-POL	3800	2200	~400
BA2-POL	2500	1400	~50

3.3. Morphology

Morphology depends both on thermodynamics and kinetics. BA2 is not much more soluble than BMA, since the methyl group is small with respect to the bisphenol A structure containing multiple EO groups, indeed the molecular weight of BMA and BA2 are 540 and 510 g/mol, respectively. However, it can be seen in Figure 3.5 that the morphology is different, with BMA having a clear porous structure while BA2 being smoother. This means that BMA either grows after phase separation has occurred or it is already separated in large domains at the spinodal decomposition. The first theory is supported by the increased solubility of the polymer in the monomer rather than in the solvent [35], that has gradually become poor at the same time, while the second is related to deswelling of the crosslinked network, that is more effective in expelling solvent [34]. Although several contributions could intervene to define the microstructure, a dominant factor can be hypothesized. The difference between BMA and BA2 lies in the polymer structure rather than the monomer because BMA is highly crosslinked, and this state of tension could contribute to deswelling [34]. One other idea involves kinetics and suggests that the faster polymerization typical of acrylates freezes phase separation process because gel point is reached quicker, when the polymer has not had enough time to arrange itself. It can be argued that BMA should reach the gelation point earlier than BA2 because it has higher ultimate T_g, and this is true for pure polymers. However, all HEs have T_gs below the curing temperature, as confirmed by conversion values. On the other hand, autoacceleration and subsequent formation of gel points is typical of acrylates [48], and it is more related to kinetics rather than thermodynamics, and this can be a potential explanation to justify incomplete phase separation of BA2.

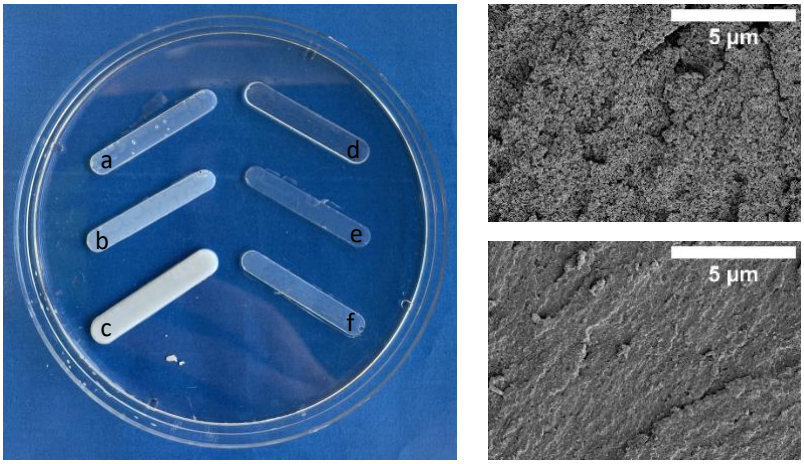

Figure 3.5. Opaqueness observed for a) BMA-E40, b) BMA-E45, c) BMA-E50, d) BA2-E40, e) BA2-E45 and f) BA2-E50, and SEM micrographs for b) and e).

A first visual observation of the cured specimens is helpful to associate the chemical structure with morphology. As can be seen in Figure 3.5, the acrylate, on the right side of the Petri dish, looks more

transparent. Moreover, it remains transparent even when the solvent concentration is increased to 50 wt% (sample f), even though a more evident shift towards an opaquer color would be expected. Instead, BMA becomes milky-white colored when containing 50 wt% solvent (sample c). The fact that BA2 does not change its opacity with solvent concentration suggests that autoacceleration hinders phase separation irrespective of the solvent amount, at least in the range between 40 and 50 wt%. Indeed, autoacceleration is a local phenomenon that is not affected by the global solvent concentration.

It has been stated in Section 2.3.6 that opaque materials contain defects in the order of the visible wavelength. However, previous researchers calculated the pores to be 10-15 nm large on average through the evaluation of the desorption isotherm after BET analysis [17], and 40-50 nm large through beam ion beam (BIB) milling coupled with SEM [16]. Even though Emilsson *et al.* (2023) used a solvent based on linear carbonates [17], Cattaruzza *et al.* (2023) employed the same solvent composition as in the present study [16]. No pore size evaluation has been conducted specifically in this research, but previous research shows an average pore size at least one order of magnitude lower than the one estimated through visual observation. Opaqueness observation is qualitative and not conclusive, but the difference with calculated values is huge. One idea to agree with the calculations is that opaqueness is provided by pore clusters rather than single pores [61]. Moreover, pore size distribution is a gaussian curve, and a fraction of pores can interact with the visible radiation.

3.4. Electrochemical properties

EIS analysis conducted on BMA shows good agreement with previous results [16]. Other researchers found a slightly higher ionic conductivity for BMA containing 39 wt% solvent ($2 \cdot 10^{-4}$ S/cm), while using a different solvent composition and lithium salt [9, 10]. In Table 3.5, average results with respective STD are represented, where the experimental ionic conductivity is the average of five measurements on BMA samples and four measurements on BA2 samples, each of them produced from two independent batches, where each batch was synthesized in different moments with slightly different relative concentrations of reagents due to weight approximation.

Table 3.5. Ionic conductivity of BMA-E45 and BA2-E45. Literature data reported from [16].

Monomer	**Measured σ (10^{-4} S/cm)**	**Literature σ (10^{-4} S/cm)**	**Difference BA2/BMA (%)**
BMA-E45	1.35 ± 0.16	1.4	-
BA2-E45	0.93 ± 0.11	-	-31%

As affirmed earlier, BA2 could be a useful HE if it were as good as BMA in conducting ions. It turns out that BA2 is around 30% worse than BMA, but it is at least in the same order of magnitude. This

means that there would be room for adjustments in the formulation to get ionic conductivities approaching BMA. At the same time, some additives and fillers are required to improve thermomechanical performance of BA2.

3.5. Conclusions about methacrylates and acrylates

BA2 shows overall lower properties than BMA. Thermomechanical properties would be acceptable for other applications, but one drawback is the glassy-rubbery transition at room temperature. It is not possible to use such a polymer in a temperature range corresponding to its glassy-rubbery transition because its properties cannot be controlled when small temperature fluctuations are present.

Another method of investigation would be the adoption of multi-acrylates, to increase the T_g and not have the glassy-rubbery transition at room temperature [62]. This aspect deals with the crosslinking density increase with crosslinker functionality. As an alternative solution, the introduction of fillers could increase the T_g as well, but the morphology would be affected. Ceramic particles, however, could be beneficial to improve interface compatibility at the electrode side [60]. On the other side, ionic conductivity could be increased by adding more solvent, but toughness and stiffness would be influenced. BA2 is more flexible and can integrate a larger amount of solvent before it becomes brittle [9], but this worsens its thermomechanical properties even more.

A feasible solution is the addition of fillers for enhancing conductivity, like carbon black (CB) or carbon nanotubes (CNTs). Yet, these fillers, together with other additives or reinforcing fillers, could heavily influence the structure, and the behavior that has been described could not be valid for more complex systems. These aspects emphasize how the conflict between electrochemical and thermomechanical properties is difficult to solve and there is no proper answer because it depends on the technical specifications that are sought to be achieved. When many variables are changed at the same time, the formulation design can only be based on a trial-and-error process rather than a robust engineering intervention.

To summarize, there is no added value given by BA2 and there is no reason for choosing it. Other couples of methacrylates and acrylates could be compared instead, but this goes beyond the scope of this work, indeed in Chapter 4 another aspect of the chemical structure is analyzed, which is more related to the thermodynamics of mixing.

4. Comparison of acrylate homopolymers

Pore size of HEs depends on solubility, that is ruled by polarity of functional groups [16]. It has been claimed that a slight increase in monomer solubility into the solvent leads to later phase separation [9], hence the solid and liquid domains cannot grow in size too much before the maximum conversion is reached, and they offer a finer microstructure consequently [16]. To keep track of the influence of the addition or removal of EO groups, two acrylates with different EO length in the chemical structure have been synthesized and compared with BA2, previously characterized in Chapter 3. In total, three acrylates, with EO=1, 2, 4, named BA1, BA2 and BA4 respectively, have been synthesized, and their monomer chemical structures are presented in Figure 4.1.

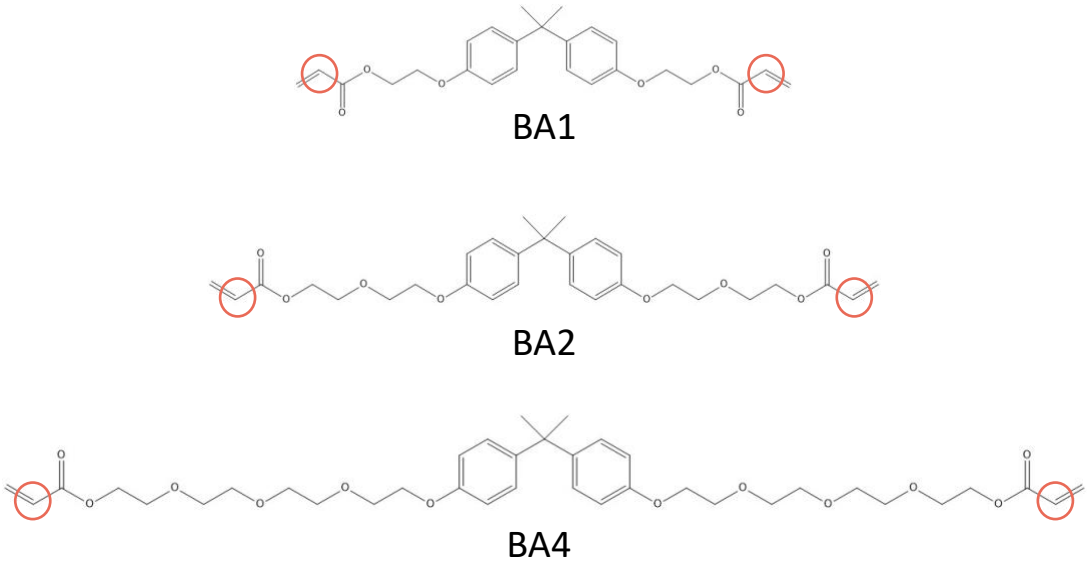

Figure 4.1. Monomer structures representing BA1, BA2 and BA4.

4.1. Previous works

Unlike the methyl side group considered in Chapter 3, the chemical change involves the monomer backbone here. In general, the introduction of EO units in the structure makes the polymer more polar because of the presence of an oxygen, that is a highly electronegative atom, connected to an ethylene structure, that is a short hydrocarbon. Moreover, EO groups are linear and increase the aliphatic contribution over the aromatic fraction, and they improve polymer flexibility. This means that both storage modulus and T_g are expected to be reduced, because crosslinking molecular weight is increased, and crosslinking density is reduced conversely [9].

Following the previous discussion, it can be stated that, while BA4 is expected to be softer than BA2 and far softer than BMA, the position of BA1 in not predictable, because the absence of the methyl groups and the presence of long EO units play a counteracting role in defining thermomechanical properties. As regards solubility, the exact values of the Hansen's parameters should be known to evaluate monomer miscibility in the solvent quantitatively. However, it can be qualitatively affirmed that BA4 is more soluble than BA2, which is in turn more soluble than BA1. Therefore, since BA2 is more soluble than BMA, it means that BA4 is far more soluble than BMA, while no conclusions can be drawn at a first evaluation from the comparison between BMA and BA1. Moreover, little information can be said about their electrical properties at first glance, under the assumption that a percolating liquid phase is formed for all formulations.

Emilsson *et al.* (2023) had already explored the effect of the addition of repeating units in oligomer solvent molecules to investigate whether the safety of HEs could be improved [17], because bicontinuous structures are made of interconnected pores and there is risk of leakage, even though in a more controlled way than LEs. It was discovered that long oligomers were more viscous and the respective HE in wet state was stiffer, while in dry state it could be seen that larger pores derived from early phase separation of long carbonates led to lower mechanical properties. There, an increase in carbonate molecular weight led to lower monomer solubility, while in this context, the introduction of EO units makes the monomer more soluble [17].

BMA and bisphenol A (EO=0) dimethacrylate, whose structures are represented in Figure 4.2 had already been widely characterized to catch the differences when EO groups are added in the monomer structure. Ihrner *et al.* (2017) discovered that the former was less soluble and led to early phase separation, thus to a more porous structure, and mechanical properties were higher because a dense network was formed [9].

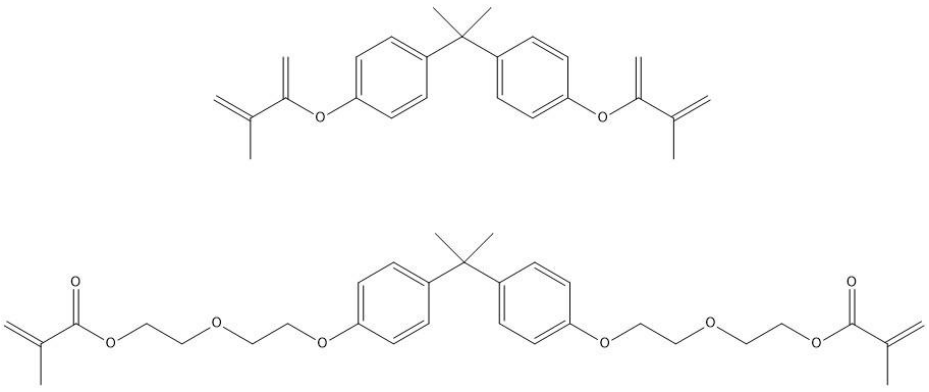

Figure 4.2. Monomer structures representing BMA and bisphenol A (EO=0) dimethacrylate. Adapted from [9].

4.2. Polymerization

All acrylate HEs studied showed high conversion after thermal curing in oven and after RT-FTIR, as demonstrated in Table 4.1, where differences were found to be negligible because they all reached conversions above 97%. It would be expected that BA4 had higher conversion than BA2 and BA1 to be the one with the lowest conversion, but this difference is not clear because of fluctuations, and these differences are expected to be marginal. RT-FTIR results are reported in Figure 4.3 averaged on two experiments performed on independent batches. It can be easily understood that conversion for pure polymers is lower because the plasticizing effect of solvent is missing. In this case, the difference between BA1-POL and BA2-POL is observed because polymerization rate is intrinsic of the type of polymer when solvent is not present.

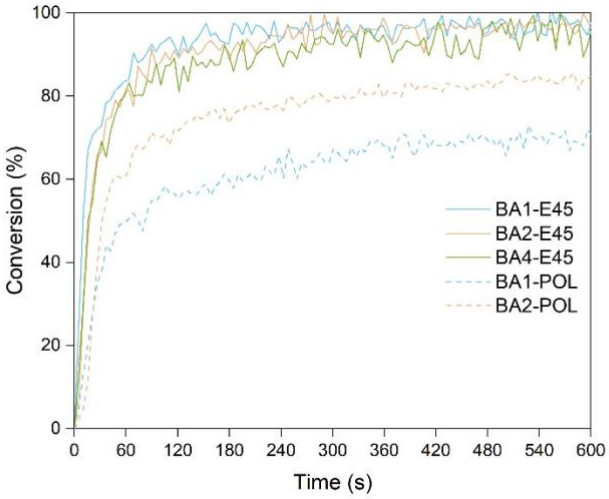

Figure 4.3. Conversion obtained from RT-FTIR analysis for acrylate homopolymer electrolytes and pure polymers.

Table 4.1. Comparison between conversion obtained after 45 minutes oven curing and 15 min RT-FTIR analysis. BA1-POL was stopped at 550 s during RT-FTIR analysis.

Polymer	**Conversion$_{\|t=45\ min}$**	**Conversion$_{\|t=15\ min}$**
BA1-E45	95	96
BA2-E45	97	97
BA4-E45	97	96
BA1-POL	80	72
BA2-POL	87	93

4.3. Thermomechanical properties

All acrylate HEs show a clear tan δ peak, while this was not the case for BMA. Tan δ curve broadness indicates high crosslinking density or heterogeneities [13]. This aspect is investigated more deeply in Chapter 5, because the copolymers presented have an intermediate behavior between BMA and the acrylates, being featured by a broad curve but recognizable peaks.

The relationship between shape of the tan δ curve and crosslinking molecular weight is justified by the fact that peaks become narrow when shifting from BA1 to BA2 and BA4, and BA4 is indeed the polymer with the highest M_c, because the monomers BA4, BA2 and BA1 have M_w=680 g/mol, 510 g/mol and 420 g/mol respectively. Ideally, at full conversion, all repeating units work as crosslinks because the monomers are difunctional. This is not completely true because of side reactions that give dangling bonds and loops, due to back-biting and intrachain reactions, but it is a good estimation to consider $M_c \approx M_w$, indeed FTIR and RT-FTIR confirm that the monomers are almost completely reacted.

The evolution of storage modulus with temperature underlines a difference between BA4 and the other HEs (Figure 4.4a). BA4 has one order of magnitude lower storage modulus at -40 °C with respect to BA1 and BA2, and it drops more quickly, so that the transition is completed already at 0 °C (Figure 4.4b). Instead, at -40 °C, BA1 and BA2 are as stiff as BMA, and a plausible explanation has already been provided in Section 3.2 in relationship with discontinuities in the material. Table 4.2 summarizes the values for storage modulus at different temperatures. At room temperature, the behavior of BA4 is predictable and, most of all, it is constant with temperature, so it could be suitable for flexible batteries. BA4 looks like a completely different material with respect to the other HEs. Further morphology investigations are carried out to classify it.

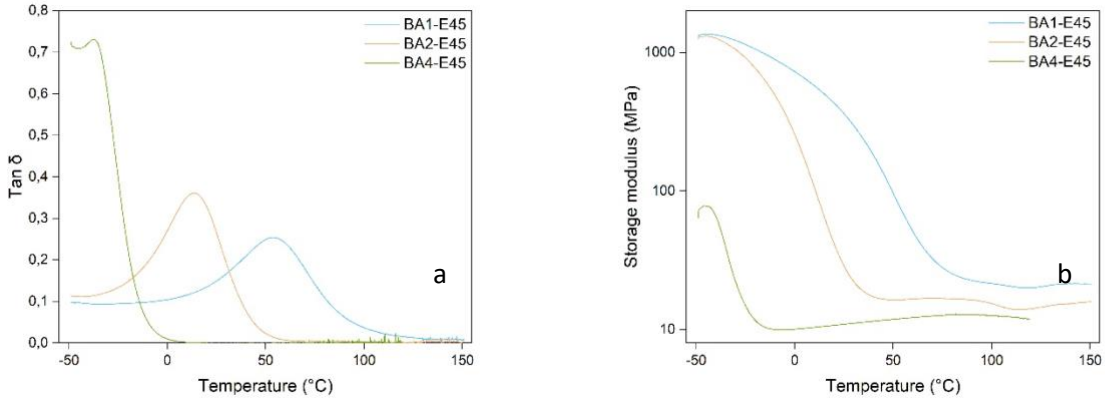

Figure 4.4. Tan δ peak (a) and storage modulus (b) for BA1-E45, BA2-E45 and BA4-E45.

Table 4.2. Storage modulus at different temperatures for BA1-E45, BA2-E45 and BA4-E45.

Monomer	**$E'_{glassy\ (T=-40\ °C)}$ (MPa)**	**$E'_{|T=25\ °C}$ (MPa)**	**$E'_{rubbery/180\ °C}$ (MPa)**
BA1-E45	1300	330	~20
BA2 -E45	1200	30	~20
BA4 -E45	60	10	~10

The fact that BMA is less stiff than the acrylates at T=-40 °C could also suggest that other transitions take place below the T_g, because the onset for BMA is at higher temperatures than BA1 and BA2, as shown in Figure S2. In reality, it seems that some transitions are activated below the onset because the curve is not flat. Examples of sub-T_g transitions are the γ-transition, which takes place when side chains start to move, and the β-transition, which is related to the coordination movement of four to eight carbons in the backbone [42]. It is reasonable that the γ-transition peak is more evident for BMA because methacrylates contain a methyl side group, while acrylates do not. These sub-T_g transitions give information about the toughness and could explain why the acrylates are stiffer [42, 63].

4.4. Morphology

Microstructure is investigated through SEM to verify whether the morphology of BA4 is compatible with GPEs. BA4 has already been studied by Kang *et al.* (2003), together with bisphenol A ethoxylate (EO=15) diacrylate, and ionic conductivity was proved to increase four-fold from EO=4 to EO=15 at room temperature [7, 64]. At the same time, since the monomer with EO=15 is expected to be more soluble in polar solvents, phase separation should be postponed, and the pores be smaller if any. Moreover, crosslinking density should be far lower than BA4 because bisphenol A ethoxylate (EO=15) diacrylate has M_w=1650 g/mol. Since it was experienced an increase in ionic conductivity from EO=4 to EO=15, there must be another mechanism for ionic conductivity, that increases when more soluble monomers are employed. A hint is suggested by the SEM micrographs in Figure 23, where BA4 looks smooth (Figure 23c) in a wide range of magnifications, between x5.00k and x40.00k. Phase separation has not proceeded extensively, and the material is a one-phase system, in particular a GPE where the crosslinked polymer is partially soluble in the solvent and integrates the liquid in its structure. In theory, the HE derived from the monomer with EO=15 should have an even smoother surface, but this material has not been analyzed here. Therefore, it can be concluded that ionic conduction throughout the bicontinuous phase is not the dominant mechanism for GPEs.

Between BA1 and BA2, the former appears more porous (Figure 4.5a) while the surface of BA2 is featured by hills and valleys (Figure 4.5b), but the pores are difficult to distinguish. This sequence of micrographs is coherent with thermodynamics regarding solubility and phase separation. Here, it is interesting to analyze whether BA2 is a phase-separated system, a gel, or a mixture of the two.

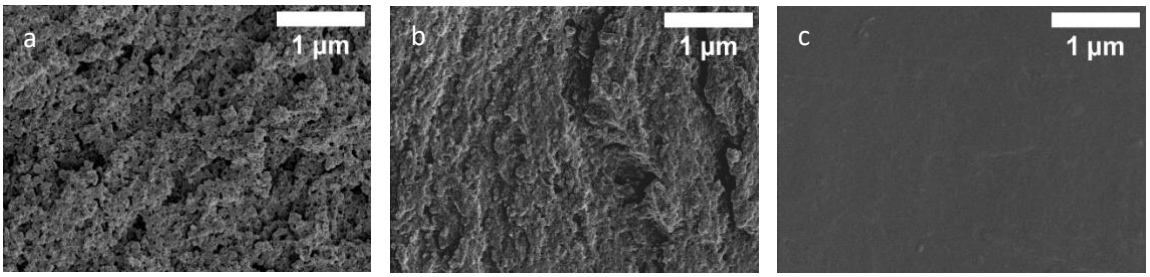

Figure 4.5. SEM micrographs for a) BA1-E45, b) BA2-E45 and c) BA4-E45.

4.5. Solvent exclusion

Solvent exclusion was carried out through leaching and vacuum drying and through vacuum drying only. Specimens are commonly soaked into deionized water before drying, but it was decided to skip leaching for a stock of specimens when it was discovered that BA4 cracked after water leaching, as illustrated in Figure 4.6 (sample f), so it was assumed that water pressure affected the polymer structure. Specimens were weighed before leaching and after 24 hours drying. Mass loss percentages are reported in Table 4.3.

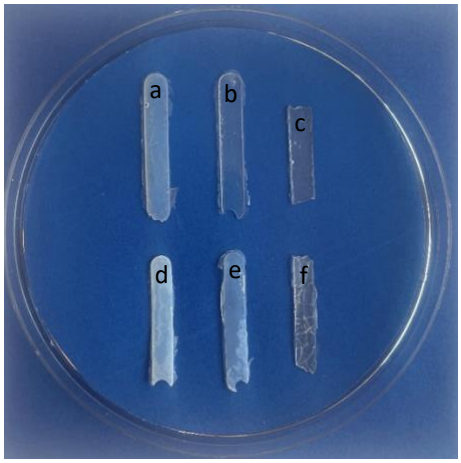

Figure 4.6. Electrolytes without leaching for a) BA1-E45, b) BA2-E45 and c) BA4-E45, and after leaching for d) BA1-E45, e) BA2-E45 and f) BA4-E45.

Table 4.3. Solvent exclusion of samples after leaching and drying and after drying only.

Monomer	Mass loss (%) Drying only	Mass loss (%) Leaching and drying
BA1-E45	23	43
BA2-E45	24	38
BA4-E45	34	45

BA4 is sensitive to leaching with deionized water because it is a soft polymer, and its structure may not be able to withstand water pressure. This experiment alone is not conclusive to establish whether the system is a one-phase gel or a bicontinuous polymer-liquid structure, but it behaves differently with respect to BA1 and BA2 because a larger amount of solvent is evaporated after 24 h only drying. This behavior is due to the solvent diffusivity towards the outside environment. Since BA4 is far softer than BA2 at room temperature, the diffusion is promoted by the action of vacuum and the network cannot retain the solvent.

BA2 retains more liquid than BA1 after leaching and drying. BA2 can be featured by close porosity or by a gel phase in combination with the bicontinuous system, but it has smaller pores than BA1. Therefore, a higher fraction of solvent volume interacts and is bound to the polymer wall [16]. However, it is not possible to exclude the hypothesis of close pores, especially because vacuum drying causes pores to coalesce and collapse.

4.6. Electrochemical properties

Ionic conductivities are compared in Table 4.4. BA2 has the lowest ionic conductivity, while BA1 and BA4 have similar values. This proves that they have different ionic conduction mechanisms, which conflict with each other when they intervene simultaneously. This is not true in general, because some systems could be found where the percolating liquid phase and the polymer flexibility work in a synergetic way.

Table 4.4. Ionic conductivity of acrylate homopolymers.

Monomer	σ (10^{-4} S/cm)
BA1-E45	1.39 ± 0.10
BA2-E45	0.93 ± 0.11
BA4-E45	1.37 ± 0.19

4.7. Conclusions about acrylates homopolymers

Acrylate homopolymers show overall lower properties than BMA. This means that the methyl side chain has a significant effect in enhancing thermomechanical properties, while the EO groups do not influence the network directly, but rather the polymerization process.

None of the acrylates is suitable for structural battery applications because BA4 is too soft, while BA1 and BA2 undergo glass transition around room temperature, 50 °C and 14 °C, respectively. On the other hand, BA1 is as conductive as BMA, so it could be improved to approach the performance of BMA. One first idea comprised the introduction of fillers, in a similar way as it has been suggested in Chapter 3, but it was decided to avoid dealing with several variables *e.g.*, type of filler, size distribution, concentration and chemical compatibility with the matrix. For this reason, it has been chosen to synthesize copolymers made of BMA and one of the acrylates in a 50/50 wt% ratio.

5. Comparison of methacrylate-acrylate copolymers

Before pointing to copolymers, one first idea was to consider a structure with one methacrylate and one acrylate terminal group, corresponding to the bisphenol A ethoxylate (EO=2) methacrylate acrylate. However, such kinds of structures are difficult to obtain through a controlled chemical reaction, and no further research was pursued. Rather, it appeared more interesting to study copolymers, from a knowledge-based and technological point of view, because copolymers are widely used in the industry *e.g.*, acrylonitrile-butadiene-styrene copolymers. It was then chosen to synthesize three copolymers derived from the combination of 50 wt% BMA and 50 wt% BA1, BA2 and BA4. These copolymers, illustrated in Figure 5.1, are named BMA-co-BA1, BMA-co-BA2 and BMA-co-BA4.

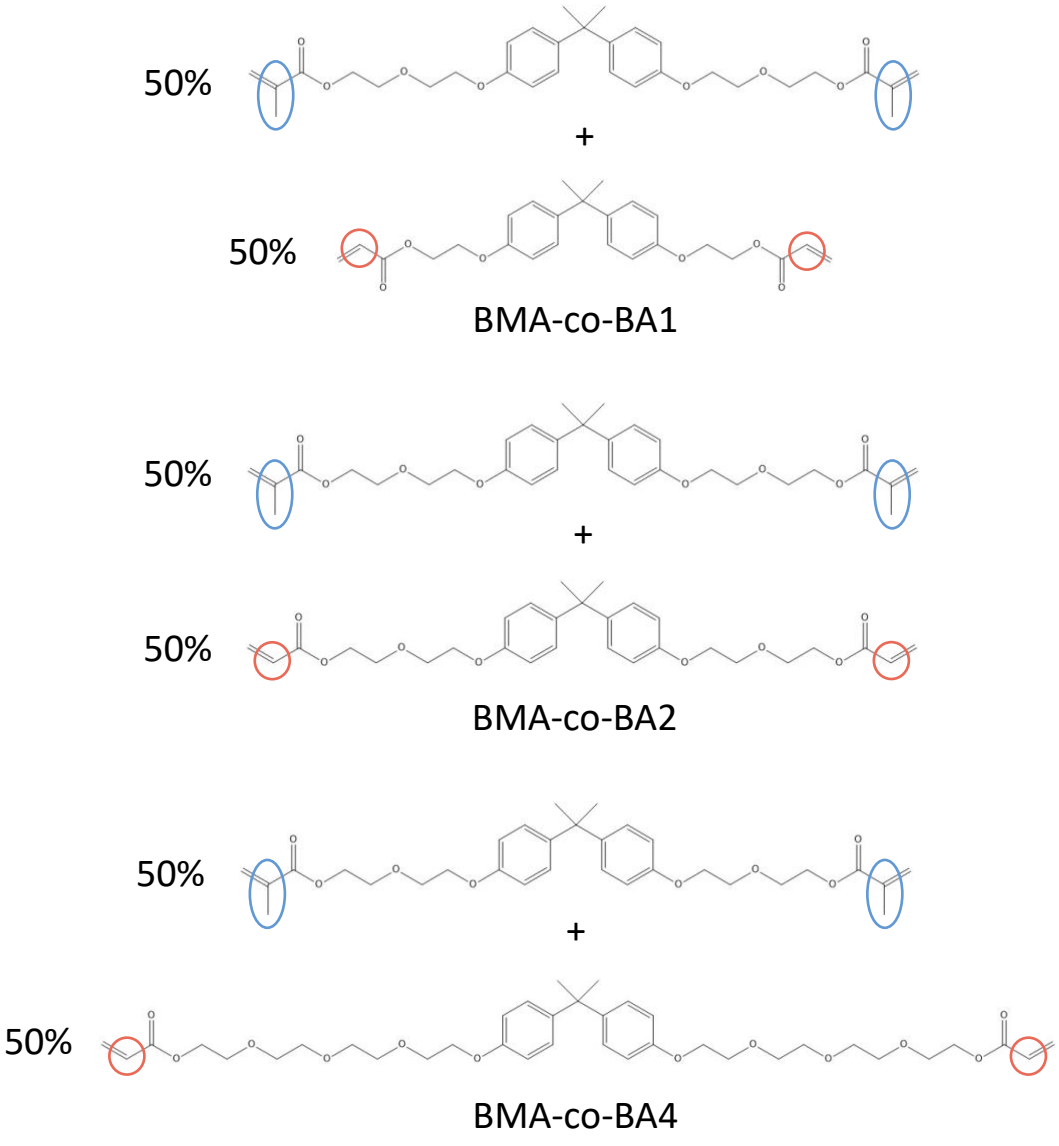

Figure 5.1. Monomer structures representing the copolymers.

Fu *et al.* (2022) have already studied copolymerization to realize GPEs for lithium batteries and obtained 37 MPa storage modulus and $4.4 \cdot 10^{-4}$ S/cm ionic conductivity for a PEGDA/BA2 copolymer GPE [65]. This material is clearly not suitable for structural batteries, but their purpose was to prevent dendrite formation at the lithium anode in LMBs.

Copolymers were synthesized under the same conditions as the homopolymers. Conversion degree after curing at 90 °C for 45 minutes is reported in Table 5.1 for both pure copolymers and HE copolymers, while the RT-FTIR conversions are shown in Figure 5.2. The same aspect discussed earlier in valid here, where HEs reach high conversions and have similar conversion rate.

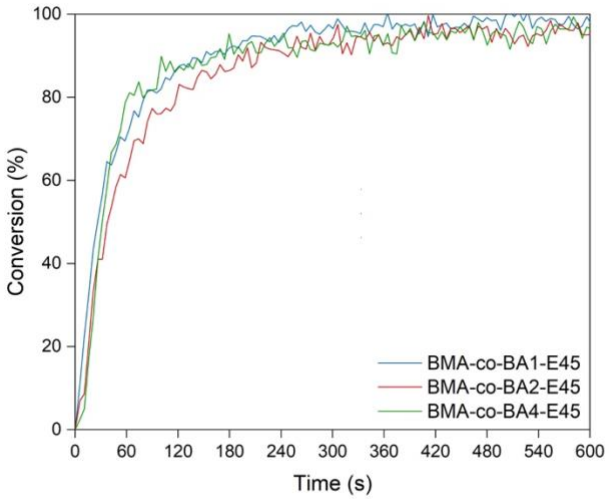

Figure 5.2. Conversion obtained from RT-FTIR analysis for copolymer HEs.

Table 5.1. Comparison between conversion obtained after 45 minutes curing and 15 min RT-FTIR analysis. BMA-co-BA1-E45 was stopped at 750 s.

Monomer	**Conversion$_{\|t=45\ min}$**	**Conversion$_{\|t=15\ min}$**
BMA-co-BA1-E45	95	98
BMA-co-BA2-E45	97	97
BMA-co-BA4-E45	98	97
BMA-co-BA1-POL	90	77
BMA-co-BA2-POL	88	77

5.1. Copolymerization

Copolymerization is the type of polymerization that involves a mixture of two monomers that react together to give a polymer containing units from both monomers [49]. The sequence of units depends on the concentration and the reactivity ratios.

In chapter 3, the rate constants have been considered for homopolymerization, where the monomers were added to a growing polymer and the radical species were of the same type. Copolymerization is different because rate constants for heteropolymerization must be considered in combination with those referred to homopolymerization.

The concept of reactivity ratios is important in copolymerization to predict the type of copolymer obtained at full conversion, *i.e.*, alternate, block or random copolymer. The reaction rates of the monomers correspond to the depletion rate of the monomers themselves, as shown in Equation 5.1-5.2, where k_{11}, k_{21}, k_{12} and k_{22} are the rate constants and depend on the thermodynamics and temperature.

$$-\frac{\mathrm{d}[\mathrm{M}_1]}{\mathrm{d}t} = k_{11}[\mathrm{M}_1\cdot][\mathrm{M}_1] + k_{21}[\mathrm{M}_2\cdot][\mathrm{M}_1] \tag{5.1}$$

$$-\frac{\mathrm{d}[\mathrm{M}_2]}{\mathrm{d}t} = k_{12}[\mathrm{M}_1\cdot][\mathrm{M}_2] + k_{22}[\mathrm{M}_2\cdot][\mathrm{M}_2] \tag{5.2}$$

Copolymer composition is given in Equation 5.3 [49], where $r_1=k_{11}/k_{12}$ and $r_2=k_{22}/k_{21}$ are the reactivity ratios.

$$\frac{\mathrm{d}[\mathrm{M}_1]}{\mathrm{d}[\mathrm{M}_2]} = \frac{[\mathrm{M}_1]}{[\mathrm{M}_2]} \cdot \frac{r_1[\mathrm{M}_1]+[\mathrm{M}_2]}{[\mathrm{M}_1]+r_2[\mathrm{M}_2]} \tag{5.3}$$

Acrylates are known to polymerize three to seven times faster than the respective methacrylates when homopolymerization takes place [62], while it is the opposite in case of copolymerization, with oligomer radicals reacting preferably with methacrylate monomers rather than acrylates [66]. This has been demonstrated by Ren *et al.* (2017) for the copolymerization at different n-butyl methacrylate-acrylate compositions through the evaluation of H-NMR spectroscopy peaks, which results are listed in Table 5.2 [46]. Dubé *et al.* (1993) had already measured the reactivity ratios for a copolymer containing methyl methacrylate and n-butyl acrylate, showing coherent results [66].

Table 5.2. Reactivity ratios for free-radical copolymerization.

Source	Monomer 1	Monomer 2	r_1	r_2	$r_1 \cdot r_2$
Ren (2017)	N-butyl methacrylate	N-butyl acrylate	2.008	0.460	0.924
Dubé (1993)	Methyl methacrylate	N-butyl acrylate	1.789	0.298	0.533
Odian (2004)	Methyl methacrylate	Methyl acrylate	2.2	0.4	0.88

If the reactivity ratios are above the unity, the radical species at the end of the growing chain prefer reacting with monomers of the same type, while it is the opposite for reactivity ratios below the unit [49]. In all cases mentioned above, reactivity ratios are above the unit for methacrylates and below for acrylates. This implies that methacrylate monomers are depleted faster and enrich the copolymer, while acrylate increases its concentration in solution [46, 66]. In this situation, a block copolymer is likely to form, especially at the very beginning of the reaction, when the methacrylate reacts preferably with the oligomer radical, and at the end, when almost only acrylate monomers are left in solution and added to the chain ends.

The product of the two reactivity ratios is related to the type of polymer obtained: when it is close to the unit, but the reactivity ratios are different from each other, it is said that they have an ideal behavior. Only when r_1, r_2=0 a random polymer is obtained. For completeness, when $r_1 \cdot r_2 \approx 0$, the obtained copolymer is alternate, while when r_1, r_2>0 a block copolymer is synthesized [49].

5.2. Thermomechanical properties

Figure 5.3 shows the storage modulus over temperature for all the copolymers and BMA, and it allows for a comparison of thermomechanical properties. Table 5.3 reports the storage moduli at three different temperatures. It is remarked one more time that the cells should be used in a range between -30 °C and 50 °C and transformations in this interval should be avoided.

With respect to homoacrylates, the drop in the storage modulus is milder. However, between -40 °C and 25 °C, the storage modulus is more than halved for all polymers, even for BMA. Anyway, there is an enormous difference with respect to homoacrylates, which experienced a drop by one order of magnitude in the same temperature interval. Since BMA is actually used as suitable electrolyte, a drop of 50% is accepted. BMA-co-BA1 behaves in a similar way, so it can be considered a good competitor. On the other side, it is risky to consider BMA-co-BA2 satisfactory because the storage modulus drops by 70%, while BMA-co-BA4 has even poorer thermomechanical properties.

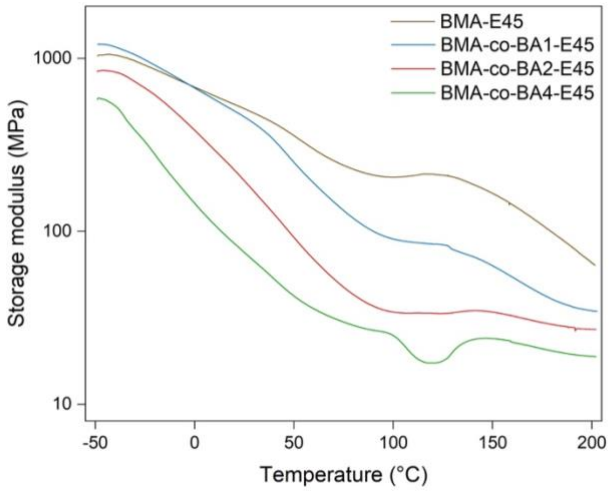

Figure 5.3. Storage modulus versus temperature on the copolymers in comparison with BMA-E45.

Table 5.3. Storage modulus at different temperatures for the copolymers and BMA-E45.

Monomer	**$E'_{glassy\ (T=-40\ °C)}$ (MPa)**	**$E'_{|T=25\ °C}$ (MPa)**	**$E'_{rubbery/180\ °C}$ (MPa)**
BMA-E45	1200	550	~200
BMA-co-BA1-E45	1200	450	~80
BMA-co-BA2-E45	800	250	~30
BMA-co-BA4-E45	500	75	~20

5.2.1. Heterogeneities

A slight decrease in the storage modulus with temperature is accompanied by a broad tan δ curve, and this is a symptom of the presence of heterogeneities, because the broadness of the tan δ peak represents how wide the temperature interval for the transformation is. If there is a large span between the onset and the offset of the curve, the temperature interval is affected by different transitions, and this suggests a heterogeneous morphology.

It can be observed from the formulations analyzed here that broad peaks only occur in copolymers (Figure 5.4) and BMA, while pure acrylates have already been shown to have narrow tan δ curves. For a better comparison, each of the acrylates has been compared with the respective copolymer in Figure S3. It seems that the narrower the peak is in the acrylate, the broader it is in the copolymer, but this observation is not conclusive, and it is not further investigated because suspected to be a coincidence.

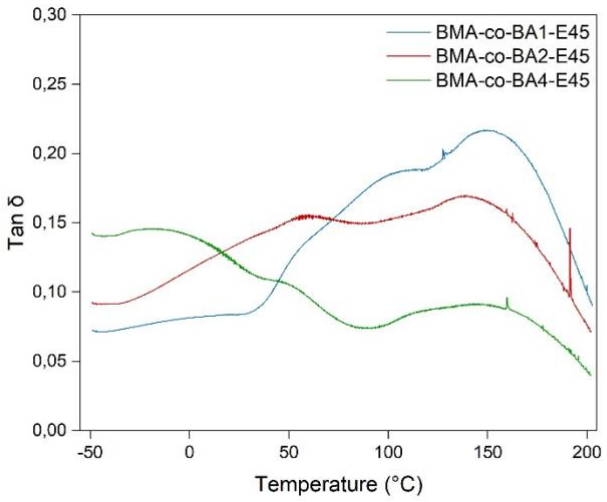

Figure 5.4. Tan δ curve for the copolymers.

To isolate the intrinsic polymer structure from the effect of post-curing, solvent evaporation and stress relaxation, DMA was also performed on dry samples [38]. Only copolymers have been analyzed in dry state, because homoacrylates showed an overall narrow tan δ curve. It is hypothesized that there might be some factors, one of which could be crosslinking density, concurring to heterogeneity of copolymers which does not affect homoacrylates instead.

It can be observed in Figure 5.5 that curves for dry samples are narrower and one peak can be recognized, but they are asymmetric and still have a tail at lower temperatures. The tan δ peak, hence the T_g value, is shifted towards higher temperatures [52], as an effect of the post-curing and solvent evaporation, that both contribute to the increase in the T_g by around 30 °C. The tan δ curve for the copolymer HEs is featured by a bimodal distribution, that can be explained considering that at 120 °C the slope for the storage modulus is inverted and the material becomes stiffer. At this temperature, the material is hardened by lack of plasticizer more than it is softened by temperature.

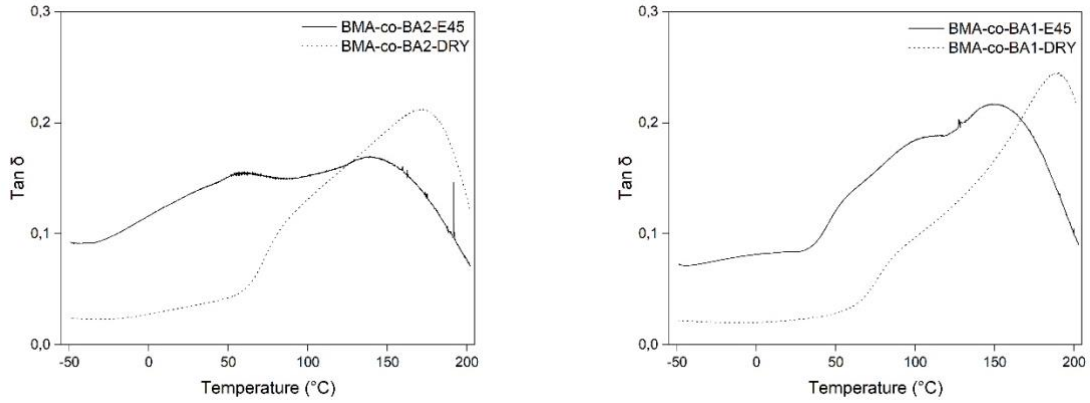

Figure 5.5. Tan δ curve for BMA-co-BA1 and BMA-co-BA2 HEs and in dry state.

In Figure S4, storage modulus comparison between electrolytes, bulk polymers, and dry samples is shown for one example. It can be observed that BMA-co-BA1-POL is softer than BMA-co-BA1-DRY above 50 °C, and this phenomenon can be explained considering that unsaturations are unexpressed crosslinks, and the material turns out weaker than the porous structure. When DMA is run twice on the same sample, as that was tried for BMA-co-BA2 for example, the T_g was increased from 95 °C to 130 °C, as shown in Figure S5.

In the literature, the main feature that is expected to contribute to inhomogeneity formation is crosslinking density [13, 48]. Three types of inhomogeneities are addressed, that are spatial density of crosslinking junctions, defects from reactions competing with the polymerization, and formation of gel clusters at the gelation point [67]. More precisely, free-radical polymerization involves homolytic cleavage of the initiator, which leaves reactive species in the solution. Monomers are featured by vinyl bonds and become activated after the initiator has partially decomposed because they are less reactive

than azocompounds. Hence, in the first stage of reaction, cyclization prevails over intermolecular crosslinking and formation of dangling bonds and loops takes place, because initiator radicals are not selective but extremely reactive. Therefore, crosslinking is localized in small regions at the beginning and leads to nanogel formation [52], because local T_g increases suddenly above curing temperature where chains are tightly crosslinked. Nanogel clusters are densely crosslinked and featured by nanometric inhomogeneities (1-10 nm), including non-uniform mesh distribution, and defects like loops and dangling bonds [67]. When polymerization goes on, intermolecular crosslinks are created, but they are loose connections with high M_c. This is called spatial inhomogeneity, and it is in the order of 10-100 nm [67]. To summarize, networks are formed by nanogels, that are nanometric entities separated from each other by spacers that are at least one order of magnitude longer [52].

In addition to the previous features, copolymers form chemical clusters where the size of the domains depends on the length of the copolymer blocks, hence the reactivity ratios [48]. The hypothesis here is that chemical clusters are constituted by the blocks in the copolymer that give locally different properties. Therefore, the reactivity should not only affect the polymerization rate, but also the microstructure, in a similar way to what was shown in section 3.3.

There is shared agreement that inhomogeneities increase with crosslinker concentration [67] and functionality [62]. These factors contribute to cyclization and the formation of nanogels separated by long spacing units [67]. In the systems studied here, monomers and crosslinkers are the same species and they are difunctional in all cases, hence there is another contributing factor for inhomogeneities, that is the crosslinking density [62].

The different behavior of methacrylates, acrylates and copolymers can be summarized by combining the discussion about heterogeneities and monomer reactivity. In copolymers, the methacrylate radical preferably adds methacrylate monomers to the growing oligomer [46], thus making the polymer rich in methacrylate and poor in acrylate. This leads to early phase separation because of deswelling [34], but only nanoclusters are formed, because few monomers have already reacted. These nanoclusters are featured by an imperfect mesh, with crosslinking units of distinct size, and defects related to chain transfer [45]. When the reaction goes on, clusters are gradually interconnected by loose constraints [68]. If the previous hypothesis is valid, in copolymers the spacers are rich in acrylate, because this species is more concentrated in the solvent, while in BMA the spacers are rich in methacrylate units and provide higher rigidity, and this can partly explain why BMA is overall stiffer than copolymers. On the other side, in pure acrylates, the forming network is not as stiff as in the other cases, and less solvent is ejected from the growing network. Consequently, gel clusters are larger, and spatial inhomogeneity is less evident.

5.2.2. Crosslinking molecular weight

Pure polymers give information about the crosslinking density because the storage modulus drop indicates how many crosslinks are released with temperature [43]. M_c values are represented in Table 5.4, where it is shown $M_c \approx 0.5 \cdot M_w$. Although the calculation is not conclusive and no comparison can be made, it is interesting to underline that M_c is in the same order of magnitude as M_w, so the relationship $M_c \approx M_w$ is partially verified.

Table 5.4. Storage modulus in the rubbery region and M_c calculated through the Equation.

Monomer	**$E'_{rubbery/180\ °C}$ (MPa)**	**M_c (g/mol)**
BA1-POL	50 at 100 °C	220
BA2-POL	50 at 100 °C	220
BMA-co-BA1-POL	55 at 150 °C	230
BMA-co-BA2-POL	70 at 150 °C	250

5.3. Electrochemical properties

Two different batches have been tested to ensure good reproducibility of the EIS technique. Six samples in total for BMA-co-BA1 and BMA-co-BA2 and three for BMA-co-BA4 were analyzed.

EIS results are reported in Table 5.5. A decreasing trend can be underlined for copolymers involving acrylates with longer EO chains. Among BMA and copolymers, three out of four electrolytes have ionic conductivity around $1.5 \cdot 10^{-4}$ S/cm, while BMA-co-BA1 is 50% more conductive.

In comparison with homopolymers, where a minimum is reached at EO=2, here the copolymer containing BA4 (BMA-co-BA4) is the least conductive, even if it is close to BMA-co-BA2. The presence of BMA in the copolymer shifts the minimum towards higher values of EO because PIPS is extended, since BMA is highly porous and gives a significant contribution to the porosity in the copolymer. This means that gel contribution in copolymers is lower than in the respective homoacrylates.

Table 5.5. Average ionic conductivity and respective standard deviation for BMA and copolymers.

Polymer	σ_{av} **(10^{-4} S/cm)**
BMA-E45	1.35 ± 0.16
BMA-co-BA1-E45	2.08 ± 0.19
BMA-co-BA2-E45	1.56 ± 0.10
BMA-co-BA4-E45	1.54 ± 0.05

5.4. Conclusions about copolymers

Results obtained in previous steps founded the basis for proposing interesting solutions that could compete with BMA. The description offered here shows that BMA-co-BA1 has passed the examination and represents a concrete alternative to BMA. The increase in electrochemical performance is not huge but it is remarkable, and the only cost is a marginally reduced stiffness at room temperature. BMA-co-BA2 and BMA-co-BA4 have acceptable properties, but it is logical to choose the best material in the perspective of future developments. BMA-co-BA1 should be tested in parallel with BMA to verify its performance during cycling, and the method for the integration of the HE in a working cell is proposed in Chapter 7.

6. Overall conclusions

Several HEs have been investigated to determine how chemistry affects phase separation. Three different steps, separated into different chapters in this work, allowed us to evaluate how methyl groups and EO units affected the polymerization process and the measurable properties. Moreover, methacrylate-acrylate copolymers were studied to investigate whether monomers can be combined to improve their properties.

Figure 6.1 shows the thermomechanical performance of all the samples analyzed. Pure acrylates are as stiff as copolymers in the glassy state, apart from BA4, that is an exception because it does not undergo PIPS. This can be explained by the fact that larger pores in copolymers reduce mechanical properties, because the solvent makes no contribution to stiffness [17]. At elevated temperatures, the state-of-the-art BMA performs the best, but copolymers can compete as they have storage moduli in the same order of magnitude. At higher temperatures, BMA and copolymers keep their stiffness better than homoacrylates because they form stronger entanglements, and a high amount of energy must be provided to untie them. Structural batteries require electrolytes with at least 100 MPa storage modulus [9] in the temperature of application. BMA and BMA-co-BA1 are well above the threshold even at 80 °C, while BA1 and BMA-co-BA2 are suitable up to 50 °C, that is a realistic temperature for applications in warm environments.

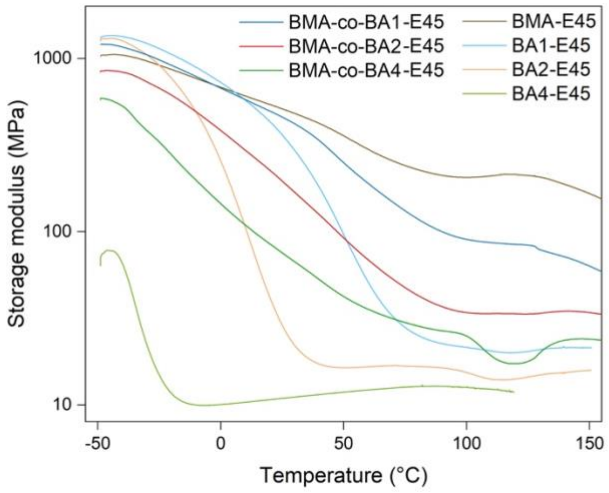

Figure 6.1. Storage modulus versus temperature for all the HEs synthetized.

One further requirement for multifunctional materials in batteries is the ionic conductivity above 10^{-4} S/cm. Figure 6.2 illustrates the electrochemical performance of all the HEs. The graph underlines three important results, that are synergetic effect of methacrylates and acrylates when combined in a copolymer, higher conductivity of the methacrylate with respect to the acrylate, at least when EO=2, and decrease in ionic conductivity for increasing EO length, both for homopolymers and copolymers. BA4 is an outliner because it has higher conductivity than BA2, even though it is more polar, thus more soluble in the solvent and featured by smaller pores consequently. In homoacrylates, ionic conductivity is increased by pore size when the system undergoes PIPS, and by polymer flexibility when the polymer is a GPE. BA2 is partially phase-separated and partially gel-like, thus this conflict makes the polymer less conductive.

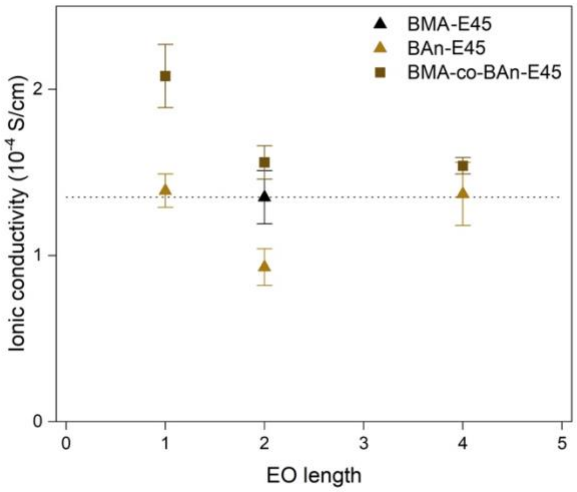

Figure 6.2. Ionic conductivity for all the samples analyzed.

What can be concluded is that the difference in ionic conductivity is not great, indeed the most conductive electrolyte is only twice as conductive as the least performing. Other types of electrolytes, like GPEs, show differences by a factor 4 when the EO length is increased from EO=4 to EO=15, from $2 \cdot 10^{-4}$ S/cm to $8 \cdot 10^{-4}$ S/cm, according to data extrapolated at 45 wt% from the graph described by Kang *et al.* [64].

There is a good match between opaqueness and ionic conductivity. In Figure 6.3 it is underlined that copolymers are opaquer than homopolymers and they are more conductive at the same time. BA1 is slightly less opaque than BMA but has similar conductivity, while BA2 is the least conductive and the most transparent after BA4, even though BA4 shows another mechanism for conduction, typical of GPEs. With this said, it can be concluded that there is a direct relationship between pore size and ionic conductivity for those systems that undergo PIPS, as previously stated by other researchers [17]. It is interesting to observe that the relationship between morphology and ionic conductivity makes possible

to guess whether an electrolyte is produced through PIPS or is a GPE because if a transparent electrolyte has appreciable electrochemical properties, as discussed for BA4, it means that pore size is less relevant than other mechanisms for conduction.

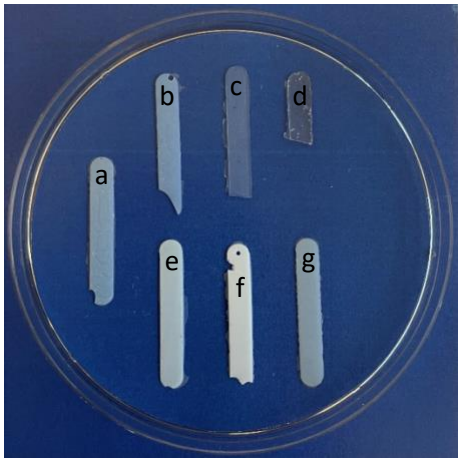

Figure 6.3. Physical appearance of HEs, where a) BMA, b) BA1, c) BA2, d) BA4, e) BMA-co-BA1, f) BMA-co-BA2 and g) BMA-co-BA4.

In the present research, bisphenol A (EO=0) dimethacrylate and bisphenol A (EO=0) diacrylate have not been studied, while bisphenol A (EO=0) dimethacrylate was characterized in some research [9]. However, if the trend is realistic, it is expected that they are more conductive than methacrylates and acrylates with one or more EO units, while the respective copolymer should be even more conductive than BMA-co-BA1.

BMA-co-BA1 is around 50% more conductive than BMA and 30% softer at 25 °C, so it is potentially the best candidate for structural battery applications. Due to the high amount of work requested and little time available, it was not possible to cycle pouch-cells with BMA-co-BA1 vacuum-infused cathodes. This remains a possibility for future research in the field.

7. Half-cell manufacturing

The feasibility of HEs must be confirmed by cycling, consisting of alternate cycles of charge and discharge, with the aim to estimate the behavior during service.

7.1. Sealed bag preparation

The process described here is valid for traditional LIBs because commercial LFP is used as a cathode instead of CFs. Irrespective of the type of cathode employed, the comparison offers a good estimation of the HE performance. A glass plate was used as support for the vacuum-infusion process, where a 15 mm-wide commercial cathode stripe (Customcells Itzehoe GmbH, 2.0 mAh/cm^2) was locked with some tape at both extremes. The glass must be carefully cleaned from dust and contaminants and the cathode stripe must be stretched not to leave spaces between the glass where the electrolyte can flow under and increase resistivity. Peel ply and fabric were applied upon the stripe and completely covered the rectangle, exceeding by at least 5 mm from each side of the electrode. The fabric promotes diffusion driven by vacuum, while the peel ply helps to detach the fabric from the cathode after vacuum infusion. Two pipes were taped on the two sides of the fabric. One of them would be connected to the vacuum pump and the other to the vial containing the electrolyte. Tacky tape was applied along the perimeter of the glass, then the cathode with the support was enveloped in a plastic bag, paying attention not to create wrinkles responsible to let the air leak in after vacuum is applied. For further safety, another bag was enveloped around, so that it could intervene if the internal bag failed. The sealed system looks as in Figure 7.1, where details of cathode, peel ply and fabric stack are highlighted.

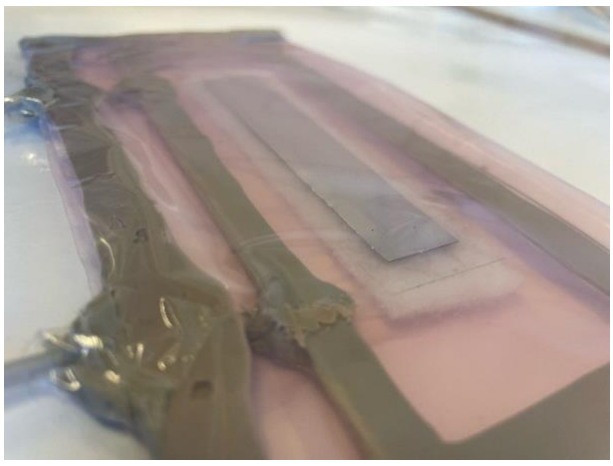

Figure 7.1. Sealed bag prepared for thermal curing.

7.2. Vacuum infusion

On an industrial scale, liquid composite molding (LCM) was revealed to be a suitable method for processing polymer-matrix composite materials. This robust process has been adapted to produce structural batteries and it proved suitable because the low viscosity helps to fill all the space and ensure a good contact with the electrode [17]. The resin was vacuum infused into a sealed bag containing the cathode and cured to get the HE [10]. At least on a lab scale, some researchers found out that the structure of specimens is homogeneous from a macroscopic point of view [9].

The electrolyte was prepared by following the steps listed in section 2.3.1, to have 3 g of monomer, and sealed in a vial. The tip of a clean vacuum-dried needle was immersed completely into the electrolyte, while the vial was tilted to guarantee immersion after some electrolyte was taken out. The pipes were clamped before the machine was turned on, then they were removed, the tube connected to the vacuum pump first to remove the remaining air present into the bag, then the tube connected to the electrolyte. The process took around one minute, and the electrode impregnation could be followed through tissue wetting. At the end, the tubes were pinched in the reverse order. The vacuum-infused cathode was heated in oven at 90 °C for 45 minutes, then introduced in the glovebox and cut into pieces of the same size as the cathodes used for the reference cells using LE.

7.3. Pouch-cell manufacturing

This process required an even cleaner space because contamination is detrimental for functionality of batteries. The materials to be integrated in the pouch-cell must lie on a foil and they must be handled with tweezers.

Lithium is found in the form of rolls. It belongs to the alkali earths, that are soft and easily oxidized materials, reactive with water and flammable. This is the reason for storing it properly. Lithium was cut into pieces 23 mm wide and at least 20 mm long. The separator was a commercial one (Whatman Pergamyn Paper 100x100 mm), made of PP. Two rectangles were obtained from the circles, longer and wither than the cathode to isolate the electrodes properly. The LE was the same used for HEs, 1 M LiTFSI in EC/PC 50/50 vol%.

The layers were stacked together in the sequence Ni current collector, Li metal anode, separator, LFP (or NMC) cathode and Al current collector. A volume of 300 µL LE was collected with a micropipette and the separator was impregnated uniformly. The electrode area must be entirely contained inside the area of the separator. The pouch cell was sealed along all the other sides and the last one with high vacuum.

In the pouch-cell containing the vacuum-infused cathode, a little amount of LE (150 µL EC/PC 50/50 vol% with 1 M LiTFSI) was added to ensure impregnation of the separator and contact with the electrodes separately. It seems questionable to add LE where HE is already present because LE

contributes to ionic conductivity by 15% and this is not considered during cycling. The cathode was infused with around 2000 mg HE and this meant that the liquid fraction weighed around 900 mg. If 150 µL liquid electrolyte are added, the total amount of solvent and salt adds up to around 1100 mg. Since ionic conductivity depends on the number of carriers, the HE provides around 85% of the contribution, while 15% is derived by LE. On an ideal picture, LE would be completely replaced, but it was revealed to be necessary to ensure that cycling was performed correctly. Figure 7.2 shows the two pouch-cells compared.

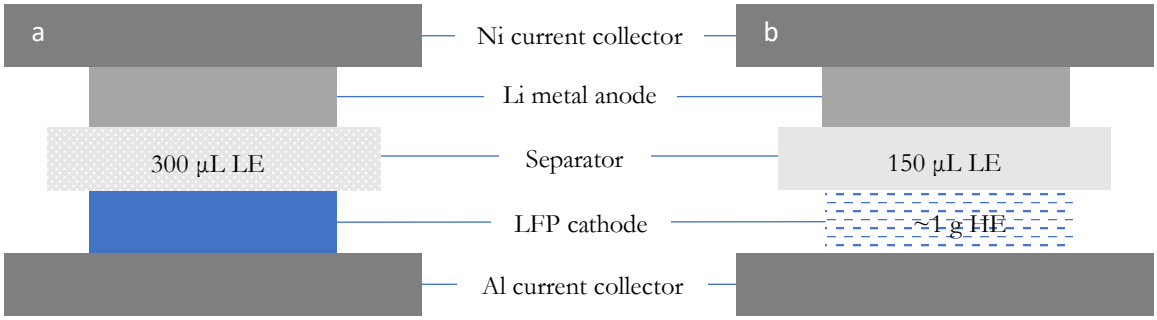

Figure 7.3. Reference (a) and testing (b) HE pouch-cell.

8. Future research

The present research was focused on a restricted variety of acrylates and methacrylates, with established solvent concentration and composition. Optimization of the formulation was not the purpose of this project, but it can be an inspiration for future research.

Batteries are sponsored as a green solution to reverse climate change, but they are not exempt from issues, for example raw material supply and recyclability. CFs for the electrodes require a sequence of high-temperature and energy consuming processes to obtain enviable mechanical properties. Moreover, solvents and electrolytes are oil-based organic compounds, while lithium salt is toxic.

Research and development for the realization of biobased CFs has already reached an advanced stage in the industry, where carbon fibers are produced from lignin, that is a biobased source, usually discarded from pulping but appreciated to be a precious biorefinery product [69].

Biopolymers contain functional groups where dipoles are created between the carbons in the backbone and highly electronegative atoms. Among the functional groups, ethers can coordinate ions, and starch, which is a polysaccharide containing glycosidic bonds between the sugar units, was revealed to effectively replace PEO in SPEs by offering even higher ionic conductivity of $3.4 \cdot 10^{-4}$ S/cm at room temperature [70]. Another research group studied the electrochemical performance of soybean proteins and found out appreciable ionic conductivity of 10^{-5} S/cm when evaporation after denaturation was conducted at T=40 °C, combined with excellent stiffness of 1 GPa, due to rigid peptide bonds and complex molecular interactions [71].

There is no deep research on biobased solutions for HEs because it is still a new field, but some ideas can be brought up for future reference. BMA has a similar structure as PEO, apart from the bisphenol A group, hence it can be hypothesized that starch could work in HEs as well. However, PIPS is sensitive to small unbalances in solubility parameters, and, in addition, the polymer phase must form a crosslinked network. Suitability of polysaccharides for PIPS is undermined because they are soluble in water and likely to be soluble in polar solvents too, and macromolecules are not crosslinked.

On the other hand, biobased crosslinkers can be found in nature or obtained through fermentation, for example, citric acid is a biomaterial derived from fermentation of cellulose sugars that is commonly used as a crosslinker. Citric acid does not contain aromatic rings, but it is trifunctional, and this helps to increase the crosslinking density reduce solubility. The effect of citric acid in the thermomechanical properties of potential HEs is unknown.

References

[1] E. C.-P. release, "Zero emission vehicles: first ‘Fit for 55' deal will end the sale of new CO2 emitting cars in Europe by 2035," 28 October 2022.

[2] B. Scrosati, “History of lithium batteries,” *Journal of solid state electrochemistry,* vol. 15, no. 7-8, pp. 1623-1630, 2011.

[3] T. Wulandari, D. Fawcett, S. B. Majumder, and G. E. J. Poinern, “Lithium-based batteries, history, current status, challenges, and future perspectives,” *Battery energy,* vol. 2, no. 6, pp. n/a, 2023.

[4] K. Edström, *Battery 2030+ Roadmap*, 2020.

[5] Y. Nishi, “The development of lithium ion secondary batteries,” *Chemical record,* vol. 1, no. 5, pp. 406-413, 2001.

[6] L. E. Asp, M. Johansson, G. Lindbergh, J. Xu, and D. Zenkert, “Structural battery composites: a review,” *Functional Composites and Structures,* vol. 1, no. 4, pp. 42001, 2019.

[7] K. Xu, “Nonaqueous Liquid Electrolytes for Lithium-Based Rechargeable Batteries,” *Chemical reviews,* vol. 104, no. 10, pp. 4303-4418, 2004.

[8] J. F. Snyder, E. D. Wetzel, and C. M. Watson, “Improving multifunctional behavior in structural electrolytes through copolymerization of structure- and conductivity-promoting monomers,” *Polymer (Guilford),* vol. 50, no. 20, pp. 4906-4916, 2009.

[9] N. Ihrner, W. Johannisson, F. Sieland, D. Zenkert, and M. Johansson, “Structural lithium ion battery electrolytes: Via reaction induced phase-separation,” *Journal of materials chemistry. A, Materials for energy and sustainability,* vol. 5, no. 48, pp. 25652-25659, 2017.

[10] L. M. Schneider, N. Ihrner, D. Zenkert, and M. Johansson, “Bicontinuous Electrolytes via Thermally Initiated Polymerization for Structural Lithium Ion Batteries,” *ACS applied energy materials,* vol. 2, no. 6, pp. 4362-4369, 2019.

[11] P. A. T. Nguyen, and J. F. Snyder, "Multifunctional properties of structural gel electrolytes." pp. 73-83.

[12] H. Zhang, S. Kulkarni, and S. L. Wunder, “Blends of POSS−PEO(n=4)8 and High Molecular Weight Poly(ethylene oxide) as Solid Polymer Electrolytes for Lithium Batteries,” *The journal of physical chemistry. B,* vol. 111, no. 14, pp. 3583-3590, 2007.

[13] M. Willgert, M. H. Kjell, E. Jacques, M. Behm, G. Lindbergh, and M. Johansson, “Photoinduced free radical polymerization of thermoset lithium battery electrolytes,” *European polymer journal,* vol. 47, no. 12, pp. 2372-2378, 2011.

[14] M. Marzantowicz, J. R. Dygas, F. Krok, J. L. Nowiński, A. Tomaszewska, Z. Florjańczyk, and E. Zygadło-Monikowska, “Crystalline phases, morphology and conductivity of PEO:LiTFSI electrolytes in the eutectic region,” *Journal of power sources,* vol. 159, no. 1, pp. 420-430, 2006.

[15] T. Eriksson, J. Mindemark, M. Yue, and D. Brandell, "Effects of nanoparticle addition to poly(ε-caprolactone) electrolytes: Crystallinity, conductivity and ambient temperature battery cycling," *Electrochimica acta,* vol. 300, pp. 489-496, 2019.

[16] M. Cattaruzza, Y. Fang, I. Furó, G. Lindbergh, F. Liu, and M. Johansson, "Hybrid polymer-liquid lithium ion electrolytes: effect of porosity on the ionic and molecular mobility," *Journal of materials chemistry. A, Materials for energy and sustainability,* vol. 11, no. 13, pp. 76-715, 2023.

[17] S. Emilsson, V. Vijayakumar, J. Mindemark, and M. Johansson, "Exploring the use of oligomeric carbonates as porogens and ion-conductors in phase-separated structural electrolytes for Lithium-ion batteries," *Electrochimica acta,* vol. 449, pp. 142176, 2023.

[18] N. Tsujioka, N. Ishizuka, N. Tanaka, T. Kubo, and K. Hosoya, "Well-controlled 3D skeletal epoxy-based monoliths obtained by polymerization induced phase separation," *Journal of polymer science. Part A, Polymer chemistry,* vol. 46, no. 10, pp. 3272-3281, 2008.

[19] S. Duan, M. Cattaruzza, V. Tu, R. M. Auenhammer, R. Jänicke, M. K. G. Johansson, F. Liu, and L. E. Asp, "Three-dimensional reconstruction and computational analysis of a structural battery composite electrolyte," *Communications materials,* vol. 4, no. 1, pp. 49-9, 2023.

[20] J. Hagberg, H. A. Maples, K. S. P. Alvim, J. Xu, W. Johannisson, A. Bismarck, D. Zenkert, and G. Lindbergh, "Lithium iron phosphate coated carbon fiber electrodes for structural lithium ion batteries," *Composites science and technology,* vol. 162, pp. 235-243, 2018.

[21] G. Fredi, S. Jeschke, A. Boulaoued, J. Wallenstein, M. Rashidi, F. Liu, R. Harnden, D. Zenkert, J. Hagberg, G. Lindbergh, P. Johansson, L. Stievano, and L. E. Asp, "Graphitic microstructure and performance of carbon fibre Li-ion structural battery electrodes," *Multifunctional Materials,* vol. 1, no. 1, pp. 15003, 2018.

[22] J. F. Snyder, E. L. Wong, and C. W. Hubbard, "Evaluation of commercially available carbon fibers, fabrics, and papers for potential use in multifunctional energy storage applications," *Journal of the Electrochemical Society,* vol. 156, no. 3, pp. A215-A224, 2009.

[23] J. Hagberg, S. Leijonmarck, and G. Lindbergh, "High Precision Coulometry of Commercial PAN-Based Carbon Fibers as Electrodes in Structural Batteries," *Journal of the Electrochemical Society,* vol. 163, no. 8, pp. A1790-A1797, 2016.

[24] E. Jacques, M. H. Kjell, D. Zenkert, and G. Lindbergh, "The effect of lithium-intercalation on the mechanical properties of carbon fibres," *Carbon (New York),* vol. 68, pp. 725-733, 2014.

[25] S. Emilsson, "Multifunctional polymer-based electrolytes for Li-ion batteries," KTH Royal Institute of Technology, 2022.

[26] A. J. Manly, and W. E. Tenhaeff, "Mechanically and thermally robust microporous copolymer separators for lithium ion batteries," *Electrochimica acta,* vol. 425, no. C, pp. 140705, 2022.

[27] Y. Yang, W. Yuan, X. Zhang, Y. Ke, Z. Qiu, J. Luo, Y. Tang, C. Wang, Y. Yuan, and Y. Huang, "A review on structuralized current collectors for high-performance lithium-ion battery anodes," *Applied energy,* vol. 276, pp. 115464, 2020.

[28] L. Cao, L. Li, Z. Xue, W. Yang, H. Zou, S. Chen, and Z. Liu, “The aluminum current collector with honeycomb-like surface and thick Al2O3 film increased durability and enhanced safety for lithium-ion batteries,” *Journal of porous materials,* vol. 27, no. 6, pp. 1677-1683, 2020.

[29] W. Johannisson, D. Carlstedt, A. Nasiri, C. Buggisch, P. Linde, D. Zenkert, L. E. Asp, G. Lindbergh, and B. Fiedler, “A screen-printing method for manufacturing of current collectors for structural batteries,” *Multifunctional Materials,* vol. 4, no. 3, pp. 35002, 2021.

[30] H. Adenusi, G. A. Chass, S. Passerini, K. V. Tian, and G. Chen, “Lithium Batteries and the Solid Electrolyte Interphase (SEI)—Progress and Outlook,” *Advanced energy materials,* vol. 13, no. 10, pp. n/a, 2023.

[31] B. Balagopal, and M. Y. Chow, “The physical manifestation of side reactions in the electrolyte of lithium-ion batteries and its impact on the terminal voltage response,” *Batteries (Basel),* vol. 6, no. 4, pp. 1-14, 2020.

[32] L. D. McIntosh, M. W. Schulze, M. T. Irwin, M. A. Hillmyer, and T. P. Lodge, “Evolution of Morphology, Modulus, and Conductivity in Polymer Electrolytes Prepared via Polymerization-Induced Phase Separation,” *Macromolecules,* vol. 48, no. 5, pp. 1418-1428, 2015.

[33] K. Dušek, “Phase separation during the formation of three-dimensional polymers,” *Journal of polymer science. Part C, Polymer symposia,* vol. 16, no. 3, pp. 1289-1299, 1967.

[34] H. M. J. Boots, J. G. Kloosterboer, C. Serbutoviez, and F. J. Touwslager, “Polymerization-Induced Phase Separation. 1. Conversion−Phase Diagrams,” *Macromolecules,* vol. 29, no. 24, pp. 7683-7689, 1996.

[35] C. Viklund, F. Svec, J. M. J. Fréchet, and K. Irgum, “Monolithic, “Molded”, Porous Materials with High Flow Characteristics for Separations, Catalysis, or Solid-Phase Chemistry: Control of Porous Properties during Polymerization,” *Chemistry of materials,* vol. 8, no. 3, pp. 744-750, 1996.

[36] N. Shirshova, A. Bismarck, E. S. Greenhalgh, P. Johansson, G. Kalinka, M. J. Marczewski, M. S. P. Shaffer, and M. Wienrich, “Composition as a Means To Control Morphology and Properties of Epoxy Based Dual-Phase Structural Electrolytes,” *Journal of physical chemistry. C,* vol. 118, no. 49, pp. 28377-28387, 2014.

[37] F. Elwinger, P. Pourmand, and I. n. Furó, “Diffusive Transport in Pores. Tortuosity and Molecular Interaction with the Pore Wall,” *Journal of physical chemistry. C,* vol. 121, no. 25, pp. 13757-13764, 2017.

[38] T. Glauser, M. Johansson, and A. Hult, “A comparison of radiation and thermal curing of thick composites,” *Macromolecular materials and engineering,* vol. 274, no. 1, pp. 25-30, 2000.

[39] A. C. Lazanas, and M. I. Prodromidis, “Electrochemical Impedance Spectroscopy□A Tutorial,” *ACS measurement science au,* vol. 3, no. 3, pp. 162-193, 2023.

[40] S. M. Sze, and K. K. Ng, "Chapter 1 Physics and Properties of Semiconductors -A Review," *Physics of semiconductor devices*, pp. 7-75, Hoboken, N.J: Wiley-Interscience, 2007.

[41] B.-A. Mei, J. Lau, T. Lin, S. H. Tolbert, B. S. Dunn, and L. Pilon, “Physical Interpretations of Electrochemical Impedance Spectroscopy of Redox Active Electrodes for Electrical Energy Storage,” *Journal of physical chemistry. C,* vol. 122, no. 43, pp. 24499-24511, 2018.

[42] K. P. Menard, and N. Menard, *Dynamic mechanical analysis*: CRC press, 2020.

[43] C. M. Blow, and I. Institution of the Rubber, *Rubber technology and manufacture*, p.^pp. 22, 527 pages illustrations 26 cm, London: Butterworths for the Institution of the Rubber Industry, 1971.

[44] J. G. Kloosterboer, G. M. M. Van de Hei, and G. F. C. M. Lijten, "Photopolymerization of Diacrylates," *Integration of Fundamental Polymer Science and Technology*, pp. 198-203, Dordrecht: Springer Netherlands, 1986.

[45] N. Ballard, and J. M. Asua, “Radical polymerization of acrylic monomers: An overview,” *Progress in polymer science,* vol. 79, pp. 40-60, 2018.

[46] S. Ren, L. Hinojosa-Castellanos, L. Zhang, and M. A. Dubé, “Bulk Free-Radical Copolymerization of n-Butyl Acrylate and n-Butyl Methacrylate: Reactivity Ratio Estimation,” *Macromolecular reaction engineering,* vol. 11, no. 3, pp. n/a, 2017.

[47] A. N. F. Peck, and R. A. Hutchinson, “Secondary Reactions in the High-Temperature Free Radical Polymerization of Butyl Acrylate,” *Macromolecules,* vol. 37, no. 16, pp. 5944-5951, 2004.

[48] K. Dusek, “Are cured thermoset resins inhomogeneous?,” *Die Angewandte makromolekulare Chemie,* vol. 240, no. 1, pp. 1-15, 1996.

[49] G. Odian, "Chain Copolymerization," *Principles of Polymerization*, pp. 464-543, United States: John Wiley & Sons, Incorporated, 2004.

[50] G. Moad, and D. H. Solomon, "Termination," *The Chemistry of Radical Polymerization*, Amsterdam: Elsevier, 2005.

[51] G. Ayrey, M. J. Humphrey, and R. C. Poller, “Radiochemical studies of free-radical vinyl polymerizations: 7. Polymerization of methyl acrylate,” *Polymer (Guilford),* vol. 18, no. 8, pp. 840-844, 1977.

[52] B. H. Jones, T. M. Alam, S. Lee, M. C. Celina, J. P. Allers, S. Park, L. Chen, E. J. Martinez, and J. L. Unangst, “Curing behavior, chain dynamics, and microstructure of high Tg thiol-acrylate networks with systematically varied network heterogeneity,” *Polymer (Guilford),* vol. 205, pp. 122783, 2020.

[53] K. Pahnke, J. Brandt, G. Gryn'ova, P. Lindner, R. Schweins, F. G. Schmidt, A. Lederer, M. L. Coote, and C. Barner-Kowollik, “Entropy driven chain effects on ligation chemistry,” *Chemical science (Cambridge),* vol. 6, no. 2, pp. 1061-1074, 2015.

[54] L. J. Hughes, and G. L. Brown, “Heterogeneous polymer systems. I. Torsional modulus studies,” *Journal of applied polymer science,* vol. 5, no. 17, pp. 580-588, 1961.

[55] S. Krause, J. J. Gormley, N. Roman, J. A. Shetter, and W. H. Watanabe, “Glass temperatures of some acrylic polymers,” *Journal of polymer science. Part A. General papers,* vol. 3, no. 10, pp. 3573-3586, 1965.

[56] C. Friedrichs, S. Emmerling, G. Kircher, R. Graf, and H. Wolfgang Spiess, "Glass transition of poly(ethylmethacrylate) admixed and bound to nanoparticles," *The Journal of chemical physics,* vol. 138, no. 12, pp. 12A503-12A503, 2013.

[57] C. E. Rehberg, W. A. Faucette, and C. H. Fisher, "Preparation and Properties of Secondary and Branched-Chain Alkyl Acrylates," *Journal of the American Chemical Society,* vol. 66, no. 10, pp. 1723-1724, 1944.

[58] J. A. Shetter, "Effect of stereoregularity on the glass temperatures of a series of polyacrylates and polymethacrylates," *Journal of polymer science. Part B, Polymer letters,* vol. 1, no. 5, pp. 209-213, 1963.

[59] M. Armand, "Polymer solid electrolytes - an overview," *Solid state ionics,* vol. 9-10, no. 2, pp. 745-754, 1983.

[60] A. Manuel Stephan, "Review on gel polymer electrolytes for lithium batteries," *European polymer journal,* vol. 42, no. 1, pp. 21-42, 2006.

[61] K. Kanamori, K. Nakanishi, and T. Hanada, "Rigid Macroporous Poly(divinylbenzene) Monoliths with a Well-Defined Bicontinuous Morphology Prepared by Living Radical Polymerization," *Advanced materials (Weinheim),* vol. 18, no. 18, pp. 2407-2411, 2006.

[62] D. L. Safranski, and K. Gall, "Effect of chemical structure and crosslinking density on the thermo-mechanical properties and toughness of (meth)acrylate shape memory polymer networks," *Polymer (Guilford),* vol. 49, no. 20, pp. 4446-4455, 2008.

[63] R. F. Boyer, "Dependence of mechanical properties on molecular motion in polymers," *Polymer engineering and science,* vol. 8, no. 3, pp. 161-185, 1968.

[64] Y. Kang, K. Cheong, K.-A. Noh, C. Lee, and D.-Y. Seung, "A study of cross-linked PEO gel polymer electrolytes using bisphenol A ethoxylate diacrylate: ionic conductivity and mechanical properties," *Journal of power sources,* vol. 119, pp. 432-437, 2003.

[65] Y. Fu, Y. Chen, and L. Zhou, "Comonomer-Tuned Gel Electrolyte Enables Ultralong Cycle Life of Solid-State Lithium Metal Batteries," *ACS applied materials & interfaces,* vol. 14, no. 36, pp. 40871-40880, 2022.

[66] M. A. Dubé, and A. Penlidis, "A systematic approach to the study of multicomponent polymerization kinetics—the butyl acrylate/methyl methacrylate/vinyl acetate example: 1. Bulk copolymerization," *Polymer (Guilford),* vol. 36, no. 3, pp. 587-598, 1995.

[67] S. Seiffert, "Origin of nanostructural inhomogeneity in polymer-network gels," *Polymer chemistry,* vol. 8, no. 31, pp. 4472-4487, 2017.

[68] S. Durmaz, and O. Okay, "Inhomogeneities in poly(acrylamide) gels: Position-dependent elastic modulus measurements," *Polymer bulletin (Berlin, Germany),* vol. 46, no. 5, pp. 409-418, 2001.

[69] A. P. Nowak, J. Hagberg, S. Leijonmarck, H. Schweinebarth, D. Baker, A. Uhlin, P. Tomani, and G. Lindbergh, "Lignin-based carbon fibers for renewable and multifunctional lithium-ion battery electrodes," *Holzforschung,* vol. 72, no. 2, pp. 81-90, 2018.

[70] Y. Lin, J. Li, K. Liu, Y. Liu, J. Liu, and X. Wang, “Unique starch polymer electrolyte for high capacity all-solid-state lithium sulfur battery,” *Green chemistry : an international journal and green chemistry resource : GC,* vol. 18, no. 13, pp. 3796-383, 2016.

[71] X. Fu, Y. Jewel, Y. Wang, J. Liu, and W.-H. Zhong, “Decoupled Ion Transport in a Protein-Based Solid Ion Conductor,” *The journal of physical chemistry letters,* vol. 7, no. 21, pp. 4304-4310, 2016.

Supporting Information

Table S1. Conversion through FTIR and RT-FTIR.

Monomer	**Conversion$_{\|t=45\ min}$ FTIR (%)**	**Conversion$_{\|t=15\ min}$ RT-FTIR (%)**
BMA-E45	93	97
BA2-E45	97	97
BMA-POL	78	68
BA2-POL	93	87

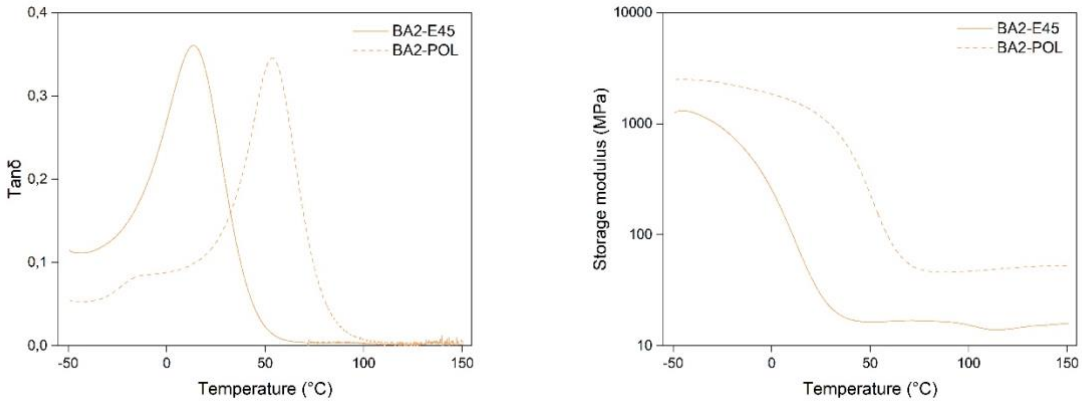

Figure S1. Storage modulus versus temperature for BA2-E45 and BA2-POL.

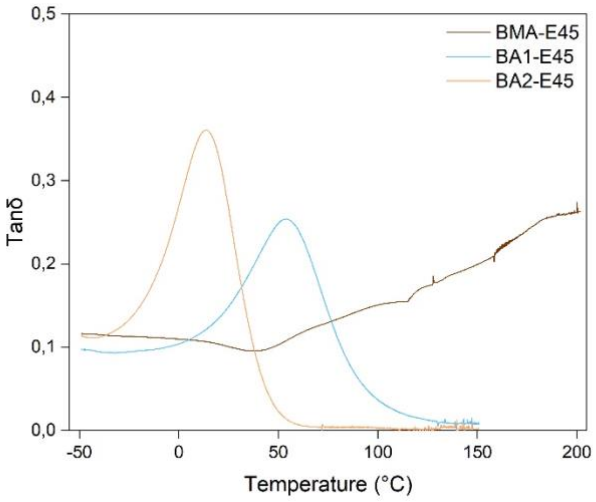

Figure S2. Storage modulus versus temperature for BMA-E45, BA1-E45 and BA2-E45.

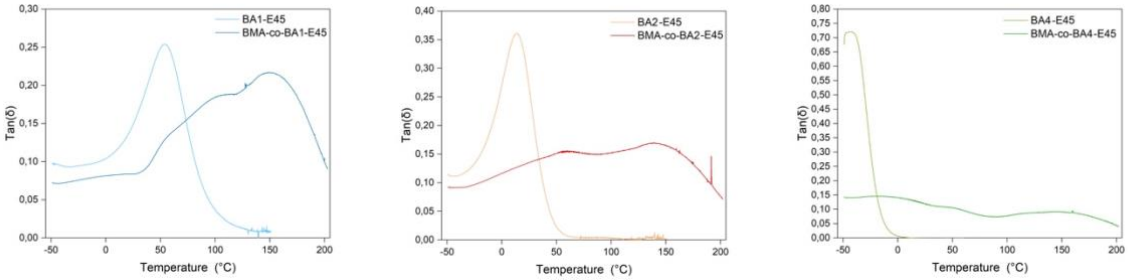

Figure S3. Tan δ curves for each acrylate and respective copolymer separately.

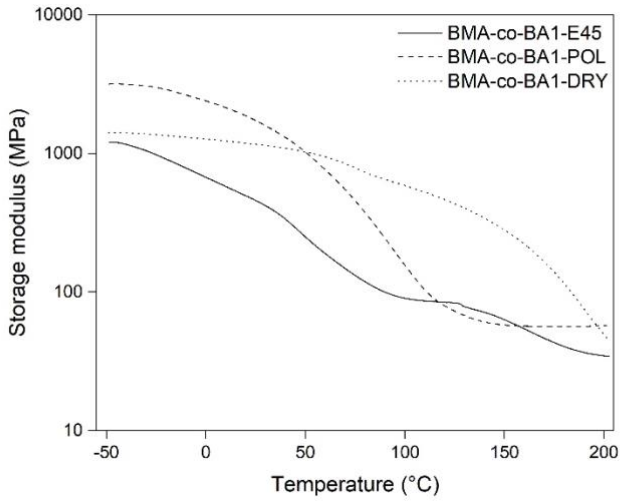

Figure S4. Storage modulus versus temperature for BMA-co-BA1 electrolyte, dry and pure polymer.

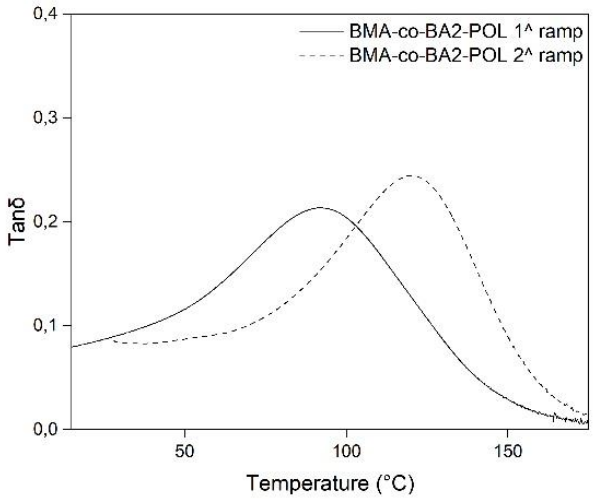

Figure S5. Storage modulus versus temperature for BMA-co-BA2-POL after the first and second temperature ramp.